Mesoscale observations of temperature and salinity in the Arctic Transpolar Drift: a high-resolution dataset from the MOSAiC Distributed Network

Mario Hoppmann[1], Ivan Kuznetsov[1,*], Ying-Chih Fang[2,*], and Benjamin Rabe[1,*]

[1]Alfred-Wegener-Institut Helmholtz-Zentrum für Polar- und Meeresforschung, Bremerhaven, Germany
[2]National Sun Yat-sen University University, 80424 Kaohsiung, Taiwan
[*]These authors contributed equally to this work.

Correspondence: Mario Hoppmann (Mario.Hoppmann@awi.de)

Abstract.

Measurements targeting mesoscale and smaller-scale processes in the ice-covered part of the Arctic Ocean are sparse in all seasons. As a result, there are significant knowledge gaps with respect to these processes, in particular related to the role of eddies and fronts in the coupled ocean–atmosphere–sea ice system. Here we present a unique observational dataset of upper ocean temperature and salinity collected by a set of buoys installed on ice floes as part of the Multidisciplinary drifting Observatory for the Study of Arctic Climate (MOSAiC) Distributed Network. The multi-sensor systems, each of them equipped with five temperature and salinity recorders on a 100 m long inductive modem tether, drifted together with the main MOSAiC ice camp through the Arctic Transpolar Drift between October 2019 and August 2020. They transmitted hydrographic in situ data via the iridium satellite network at 10 minute intervals. While three buoys failed early due to ice dynamics, five of them recorded data continuously for 10 months. Four units were successfully recovered in early August 2020, additionally yielding internally stored instrument data at 2 minute intervals. The raw data (Hoppmann et al., 2021i) were merged, processed, quality-controlled, and validated using independent measurements also obtained during MOSAiC. The finally processed dataset is publicly available under Hoppmann et al. (2022i). As an important part of the MOSAiC physical oceanography program, this unique dataset has many synergies with the manifold co-located observational datasets and is expected to yield significant insights into ocean processes, as well as to contribute to the validation of high-resolution numerical simulations. While this dataset also has the potential to contribute to submesoscale process studies, this paper mainly highlights selected preliminary findings on mesoscale processes.

1 Introduction

Oceanic mesoscales host a variety of important features and processes that have been extensively studied during the past four decades, pioneered by the Mid Ocean Dynamics Experiment in the 1970s (MODE, Bretherton et al., 1976; Jochum and Murtugudde, 2006; McWilliams, 1976). Mesoscale processes are characterized by horizontal scales of few to several tens of kilometers and temporal scales much greater than the local inertial periods, up to the order of one month. An important

consequence is that the vertical velocities are 10^3 to 10^4 times weaker than the horizontal velocities (Thomas et al., 2008). The mesoscales are the major contributors in terms of the kinetic energy reservoir (Ferrari and Wunsch, 2008) and usually manifest in the form of geostrophic eddies that are shown ubiquitously in present-day satellite imagery (McGillicuddy, 2016). Their occurrence has been linked to concurrently occurring tilted isopycnals (Gill et al., 1974), where baroclinic instabilities submesoscale release of potential energy which generates eddies. Global estimates of mesoscale eddy variability indicate that mesoscale eddies can be correlated with the first mode baroclinic Rossby radius (Chelton et al., 1998; Smith, 2007). In the Arctic Ocean, recent studies have highlighted the role of mesoscale eddies and the significant fraction that eddy kinetic energy contributes to total kinetic energy in observations (Zhao et al., 2014) and high-resolution numerical simulations (Wang et al., 2020). At the same time, eddies have likely been historically underestimated in key regions of the Arctic Ocean (Porter et al., 2020).

Apart from the mesoscales, recent advancements in instrumentation and computing power have allowed us to appreciate further the submesoscale regime, which resides between the mesoscale and turbulence (McWilliams, 2016). Submesoscales are characterised by O(1) Rossby and Richardson numbers, and evolve with relative shorter spatial O(100 m to 10 km) and temporal O(days) scales. Mesoscale and submesoscale processes both feature non-negligible vertical velocities (D'Asaro et al., 2011; Thomas et al., 2008) that make them unique in bridging the momentum exchange between the ocean surface layer and the interior underneath (e.g. Lévy et al., 2018). Numerical simulations have shown that shifts from mesoscale to submesoscale regimes (Capet et al., 2008) result in frontal instabilities (e.the g. Mahadevan, 2016; Mahadevan et al., 2010) and secondary ageostrophic circulation (Thomas, 2005). In the Arctic basin, mesoscale and submesoscale variability does not only occur under seasonal ice cover and in the MIZ (e.g. Gallaher et al., 2016) but also under perennial sea ice. Although eddy activity is lower in the central Arctic than near the boundaries, the portion of total kinetic energy due to mesoscale eddies (eddy kinetic energy) is significant in the central Arctic Ocean (Zhao et al., 2014; Wang et al., 2020; von Appen et al., 2022). The local processes acting at the mesoscale and smaller scales not only alter the local hydrography and circulation but also feedback to the large scale. State-of-the-art climate and earth system models would benefit from advancing our knowledge of these processes and improving parameterization (Hewitt et al., 2020).

Although present-day field campaigns may be able to observe mesoscale currents and features by remote sensing at lower latitudes (Gaube et al., 2015) and as part of carefully-planned synoptic surveys (Huang et al., 2018), high latitudes pose a greater challenge. In the Arctic basin, mesoscales shrink to an order of 5 to 20 km (Nurser and Bacon, 2014; D'Asaro, 1988; Manley and Hunkins, 1985) from those of 50 to 100 km at mid-latitudes (e.g. Smith, 2007). Observations of the mesoscale by remote sensing are limited in the central Arctic by seasonal and perennial ice cover, though plans for dedicated satellite missions exist to cover even the submesoscale (e.g. Gommenginger et al., 2019). Ship-based surveys in the central Arctic Ocean can give a good impression of the large-scale state and interannual changes. However, observations of mesoscale processes remain a challenge due to the scales involved and the typically synoptic design of hydrographic surveys. In addition, they are limited by logistical constraints and the high cost of operation in the pack ice to the melting season and early freeze-up, from about June to September. Further, towed or autonomous platforms, such as AUVs or gliders, remain difficult or impossible to operate in the central Arctic ice pack. Similar constraints apply to seafloor moorings (e.g. Zhao et al., 2016).

One way to overcome these constraints is the use of ice-tethered drifting ocean observing platforms. During the past three decades, these have increasingly facilitated in situ observations to augment ship-based surveys. Examples include the Polar Ocean Profiling System (POPS, Kikuchi et al., 2007), the Ice-tethered Profiler (ITP, Toole et al., 2006), and the Ice–Atmosphere–Ocean Observing System (IAOOS) platforms (Koenig et al., 2016; Athanase et al., 2019). Providing year-round time series in the Transpolar Drift and the Canada Basins, they are usually aimed at large-scale monitoring, with efforts such as the Marginal Ice Zone program in the Canada Basin (Lee et al., 2017) being the exception. Coordinated efforts particularly aim at vertically connecting the processes in the realms of the atmosphere, sea ice, and ocean. However, most deployments are not aimed at resolving the mesoscale in the horizontal. Several systems have contained components that were designed to measure temperature and salinity at a high frequency to capture short-term fluctuations, such as those associated with submesoscale, mesoscale and internal wave variability. Examples are again the WHOI ITP (Toole et al., 2006), the JAMSTEC-Compact Arctic Drifter buoys (J-CAD, Hatakeyama et al., 2012), as well as the UpTempO (Steele, 2017) and WARM buoys (Hill et al., 2019) .

The details of mesoscale processes and their effect on water mass formation, local circulation, and fluxes need to be known to understand changes on an Arctic-wide scale; in particular, with respect to the variety of feedbacks between the ocean and the sea ice, as well as the atmosphere (e.g. Zhao et al., 2016). The current lack of knowledge and incorrect representation of vertical mixing processes in climate models result in large biases in Arctic Ocean temperature and salinity (Ilicak et al., 2016) and limit our knowledge of their effect on large-scale circulation (Timmermans and Marshall, 2020). The magnitude of the mesoscale (e.g. Nurser and Bacon, 2014; Zhao et al., 2014) indicates the potential to detect associated ocean features with novel, autonomous in situ platforms, given the quasi-synoptic character of observations from drifting sea ice.

Here we present a unique observational dataset from the central Arctic Ocean obtained as part of the physical oceanography work program during the Multidisciplinary Observatory for the Study of Arctic Climate (MOSAiC) experiment in 2019/20 (Rabe et al., 2022). We designed and deployed an autonomous buoy array equipped with several oceanographic sensors upstream in the significantly understudied albeit crucially important Arctic Transpolar Drift, that can resolve processes on the mesoscale over a full seasonal cycle. Below we outline the concept, realization, data processing, and -validation, as well as discuss environmental, technical, and analytical challenges. We present exemplary results to showcase the potential for an analysis of mesoscale variability and conclude with an outlook on the wider scope of this unique dataset, including the potential use for the study of submesoscale processes such as restratification or internal waves.

2 Material and methods

2.1 General concept

To address some of the knowledge gaps outlined above, a set of eight buoys carrying a suite of oceanographic sensors was deployed upstream in the Transpolar Drift in October 2019 as part of the MOSAiC Distributed Network (DN). The instruments were installed within ~ 40 km of the German research icebreaker RV *Polarstern*, which was planned to stay anchored to the same ice floe for an entire year and constituted the main MOSAiC ice camp (also referred to as "Central Observatory"). Incorporating a diverse collection of autonomous instrumentation, the DN was intended to spatially extend and complement

the extensive work program conducted by the different teams (Nicolaus et al., 2022; Shupe et al., 2022; Rabe et al., 2022) in the Central Observatory, and to bridge the gap between the spot measurements and larger-scale airborne and satellite observations. The DN consisted of several complex instrument systems distributed to a dozen main sites, complemented by a large number of additional simple GPS buoys in the wider DN. Eight of these sites were equipped with the buoys presented in this study, each co-deployed with a handful of other instruments (see below). This distribution, together with the ice drift, covered the mesoscale (of the order of a few tens of kilometers), and to some extent the submesoscale (of the order of 1 km). While we were originally aiming for less spacing between the individual buoys to better resolve the submesoscale processes, the challenging ice conditions and absence of sufficiently stable floes required us to change the plan and extend the deployment area to reduce the risk of early failures. The exceptionally dynamic ice pack in winter 2019/20 led to a failure of several other buoys in the early period of MOSAiC (including 3 of 8 units described here, see 2.3).

Our focus was on the upper water column, in particular, the whole upper ocean mixed layer across most of the Eurasian Basin. The primary aim of the expedition was to capture local processes in the strongly stratified region of the Transpolar Drift, which features near-surface waters much fresher and colder than those found in the Nansen Basin close to the inflow of water of Atlantic origin. The drift started in the Amundsen Basin as close to the Siberian shelves as possible, where the Transpolar Drift stream originates. That allowed a continuous drift into late spring without relocating the ice camp, and with a chance to recover the buoys. Placing instruments in the upper 100 m was expected to capture processes in the seasonally deepening and subsequently restratifying mixed layer, and to also cover part of the upper halocline throughout much of the year.

We required a sufficient number of measurement points in the vertical to give a good indication of the structure of the mixed layer and the upper halocline. This is especially aimed at resolving passing eddies or fronts, whilst minimizing the number of sensor packages and associated costs. Deployment alongside ocean profilers at different sites within the DN, such as the Woods Hole Ice-Tethered Profiler (Toole et al., 2006) or the Drift-Towing Ocean Profiler (Ocean University of China, 2021), ensured that the vertical structure of the upper water column was measured to 1 dbar resolution at least once a day. At the same time, our systems aimed at capturing transient phenomena, such as internal waves or eddies, requiring measurements as frequent as two minutes.

2.2 Instrument description

The sensor platform, hereafter referred to as "Salinity-Ice-Tether" (SIT), is a floatable buoy built by Pacific Gyre (California, USA) and comprised an oval surface float that housed the main electronics and batteries, connected to a 100 m long inductive modem cable with a 10 kg terminal weight attached to the bottom (Fig. 1a). Along this tether, five SBE37IMP MicroCAT CTDs built by SeaBird Scientific, California, USA, and hereafter referred to as "CTDs" (Conductivity–Temperature–Depth), were mounted at depths of 10, 20, 50, 75, and 100 m. Following the naming convention of the general AWI buoy program, which was also implemented for all MOSAiC buoys, we identify the individual buoys by an ID consisting of the deployment year (in this case "2019"), followed by a buoy type-specific letter (in this case "O") and a running number (here, "1" to "8"). The corresponding buoy IDs are 2019O1 to 2019O8 for the eight SIT systems. Furthermore, we refer to the individual CTDs

by the buoy ID and the nominal CTD deployment depth, i.e. 2019O1-10m is the CTD attached to the tether of buoy 2019O1 at a nominal depth of 10 m.
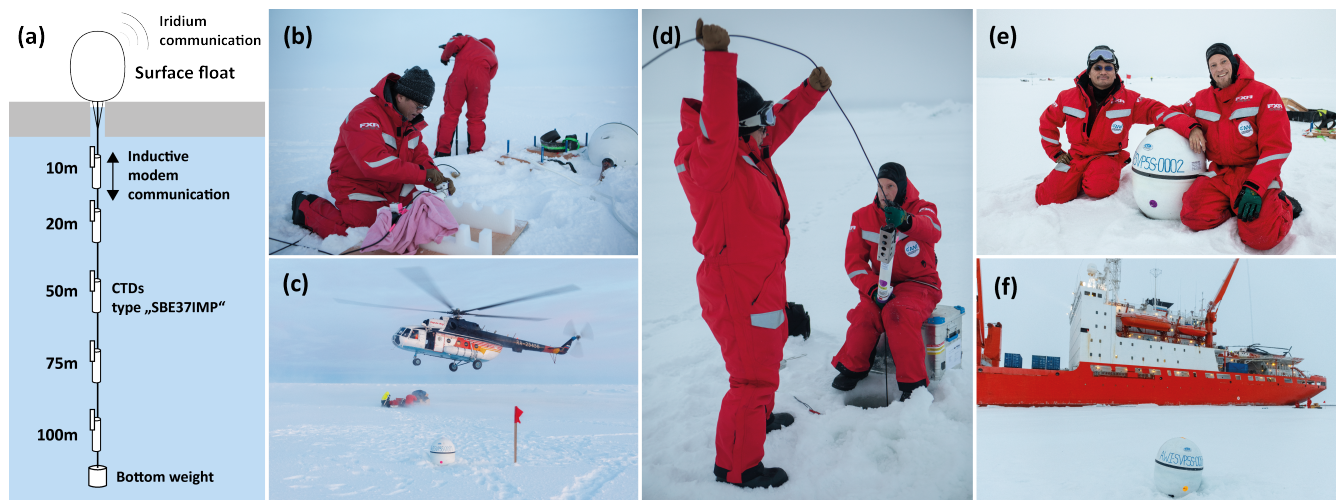
Figure 1. Salinity Ice Tether buoy schematic (a) and deployment photos (b-f).

To ensure an operational time of ∼1 year, the individual CTDs were set to record data internally at 2 minute intervals, independent of the buoys' own sample and transmit intervals. The surface buoy itself recorded GPS position and surface temperature and carried a submergence sensor. Furthermore, the buoy controller polled all CTDs for an additional measurement according to a pre-configured buoy sampling interval, which could in principle be adjusted by sending a reconfiguration command via iridium if necessary. However, throughout our experiment, all buoys were set to take a measurement and immediately transmit the corresponding data at a fixed 10 minute interval, chosen to ensure an operational time of the surface buoy of at least one year. In summary, the internal sampling interval of the CTDs was 2 minutes, while an additional CTD measurement was obtained and transmitted by the buoy every 10 minutes together with the corresponding auxiliary (meta)data.

Upon removal of a magnet at the side of the hull after deployment, the buoy was switched on and automatically activated the internal 2 minute sampling of the attached CTDs. The buoy controller sampled all of the CTDs one minute before a scheduled transmission. After reading the auxiliary sensors, the buoy controller sampled the GPS at the scheduled transmit time to get a valid GPS position for transmission. The data resulting from this measurement cycle were then compressed into a file and sent via the Iridium short burst data (sbd) protocol to a shore-based server, which decoded the data and provided the data for download. In the standard buoy firmware, pressure is by default rounded to 0.1 dbar before transmission to save data size and transmission cost. Unfortunately, this could not be changed during operation. Salinity was calculated on the server side based on the transmitted temperature, conductivity, and pressure measurements according to the Practical Salinity Scale 1978 (PSS-78). For the final dataset, however, practical salinity was recalculated from these variables using the Matlab GSW Toolbox Version 3.05.5 (McDougall and Barker, 2011).

The SBE37 MicroCAT CTD itself (either in its normal or inductive modem configuration) is a reliable and accurate sensor
that has been used for studies of physical oceanography on various platforms all over the world for decades; in particular, for
moored operations (e.g. Beszczynska-Möller et al., 2012). The stated initial accuracy for this sensor type is ± 0.003 mS cm^{-1}
for conductivity, $\pm 0.002°$C for temperature and ± 0.1 % of the full scale range for pressure. For our instruments, the pressure
rating was between 100 and 1000 m due to the limited availability of 100 m pressure sensors at the time of manufacturing. The
initial accuracy for a 100 m calibrated pressure sensor (0.1 % of the full scale range) is thereby $\sim$0.1 dbar. As stated earlier,
the buoy firmware only transmitted 10-minute pressure records to the first decimal, resulting in a vertical resolution of 0.1
dbar compared to 0.02 to 0.002 dbar (0.002 % full scale range) of the CTDs themselves. Since the accuracy is on the same
order of magnitude, we do not consider the transmission limitation for pressure as significant in relation to our final dataset.
For datasets that include the internally recorded data of the recovered CTDs, the pressure records as sent by the buoy have been
interpolated to improve their quality (see Section 3). The typical sensor stability is rated as 0.003 mS cm^{-1} and 0.0002°C per
month for conductivity and temperature, respectively, and 0.05 % of the full scale range (pressure) per year.

2.3 Field deployment and recovery

The buoys were deployed along with a suite of other platforms during the setup phase of the MOSAiC Distributed Network
by the Russian icebreaker *Akademik Fedorov* in early October 2019Toolbox1b-f). A few days before reaching the deployment
destination, the instruments were successfully tested on deck. Ice floes were selected based on an inspection of high-resolution
satellite imagery and helicopter surveys. The ice conditions were challenging for permanent installations since thin ice was
predominant in the deployment area (Krumpen et al., 2020). The station work was either done from the ship or by MI-8
helicopters. The instruments were co-installed on selected ice floes together with SIMBA-type ice mass balance buoys (Jackson
et al., 2013), Snow Buoys (Nicolaus et al., 2021a), and D-TOP Ocean Profilers.

The Snow Buoy, SIMBA, and SIT buoys were installed close to each other, while the D-TOP was installed at a distance of
at least 70 m away. After a deployment site with sufficiently stable level ice was chosen, the buoy tether was laid out on the
ice, and the CTDs were attached to their designated depth positions along the cable. The instruments were covered with towels
for protection during handling on the ice and snow. the cable and instruments were manually lowered into the ocean through a
10 inch diameter hole in the ice, and the surface float was placed on top of the hole. Air temperatures were as low as -15°C .
Table 1 summarizes the deployment information for each instrument.

The trajectories of the buoys during their 10 months long drift are presented in Section 4.2. 2019O2, 2019O7, and 2019O8
failed within the first 5 weeks after their deployment. 2019O5 failed in July 2020, most likely due to ice ridging, having
survived for 9 months. The other four buoys were recovered from the decaying ice field in the marginal ice zone of Fram Strait
in August 2020 by the German and Russian icebreakers RV *Polarstern* and *Akademik Tryoshnikov*.

Table 1. Buoy deployment and recovery metadata.

Buoy ID	Site	Deployment Date	Lon	Lat	Last data	Lon	Lat	Days
2019O1	M1	20191005T05:10	131.27	84.92	20200805T10:00	-1.54	78.59	305
2019O2	M2	20191007T02:40	135.76	84.87	20191113T22:50	120.14	85.95	40
2019O3	M3	20191007T07:20	137.83	85.05	20200803T12:20	-4.35	78.63	301
2019O4	M4	20191008T01:30	136.28	85.11	20200814T07:10	-8.53	80.13	311
2019O5	M5	20191009T02:50	139.05	85.05	20200712T15:50	-1.69	81.32	278
2019O6	M6	20191010T03:20	133.23	85.13	20200813T13:40	-7.49	80.25	308
2019O7	M7	20191011T02:40	135.84	84.74	20191025T20:20	128.36	85.32	15
2019O8	M8	20191011T01:30	134.50	84.99	20191025T20:50	126.32	85.55	15

3 Data processing & quality flags

In this paper, we exclusively refer to in situ temperature (T in °C) and practical salinity (S in PSU), if not stated otherwise. The final data collection consists of eight individual datasets, one for each buoy. Four are merged products of the initially iridium-transmitted buoy data (10 minute interval) and the corresponding CTD data from recovered instruments (2 minute interval). To ensure the highest possible data quality and at the same time leave the end user the possibility to apply his/her own quality checks, we decided to not entirely remove questionable data, but instead apply a primary quality flagging scheme to the oceanographic data in a modified version of the scheme proposed in UNESCO-IOC (2013). The primary level flagging scheme we use here is composed of five quality values which are defined as follows: 1 — good, 2 — modified, 3 — questionable, 4 — bad, and 9 — missing data. The difference from the originally proposed scheme is that "2 — not evaluated" was replaced by "2 — modified", as we think it should be general practice to evaluate all data points. In some cases, as also described below, the quality of the data could be improved by modification of the original record, indicated by the "2 — modified" flag. We applied this scheme to the oceanographic data only. We decided against using an additional, secondary flagging scheme, as further discrimination of the quality checks described below would not provide any substantial added value to our data.

Each dataset was compiled in the following way: First, the buoy data was obtained from the Pacific Gyre web server. A handful of obvious GPS outliers were removed and the gaps were filled by linear interpolation. Buoy drift speed was calculated from the difference between adjacent GPS positions. The resulting drift speeds were consistent throughout, and no further processing was applied. Surface temperature data was controlled for plausibility mainly by a general range check, and no correction was necessary. The polled sampling of the CTDs was initiated by the buoy one minute before the acquisition of GPS position and time. For consistency and simplicity, we used the time of CTD sampling as the general timestamp (rather than the GPS fix one minute later), accepting an additional uncertainty in the GPS position of <30 m, depending on the drift speed. If higher temporal resolution CTD data was available for a particular buoy, both datasets were merged (see below). No quality

flags for position or surface temperature are given since their quality is overall good and the oceanographic measurements are the focus of this observational dataset. Data from the 20 recovered CTDs (corresponding buoy IDs: 2019O1, 2019O3, 2019O4, and 2019O6) were downloaded using the Seaterm V2 software (Version 2.8.0.119) by Seabird. For logistical reasons, data from 2019O1 and 2019O3 were downloaded at sea as .cap files, whereas data from 2019O4 and 2019O6 were recovered at home after the end of MOSAiC as standard .hex, .xml and .xmlcon files and converted to .cnv files using the Seabird software SBEDataProcessing (Version 7.26.7).

The CTD timestamps were checked for consistency using distinct features in the pressure records of each set of CTDs installed on any given buoy (for example when all instruments would be lifted at the same time due to an increased drift speed as a result of strong winds). 2019O4-75m was mistakenly configured to a 30 s measurement interval, which led to an early power failure (see below). For this CTD, only every fourth record was used for the final dataset for consistency reasons. The full dataset is however still available in the raw data archive. Also, the instrument time of 2019O4-75m had an offset of 56s, which was corrected.

For the four merged data products, the data were combined and reordered based on their timestamps. All records before the deployment have been removed from the dataset (not flagged) based on the pressure record of the instruments. In some instances, the initial conductivity values appeared suspiciously low, sometimes even with sudden jumps to higher values. There is a high probability that these are erroneous records caused by ice formation in the pump or conductivity cell. This could have been caused by the instrument being exposed to cold air temperatures before deployment through the ice. In most instances, this effect disappeared after a few days to several weeks. We tried to identify a point in the time series where the salinity data starts to become reasonable; for example, after the last suspicious jump, by plausibility checks and comparison against adjacent CTDs, or comparison to other buoy data. After a specific point in time was identified from where the data seemed plausible, we flagged all prior records as "3 — questionable". Temperature and pressure records were not affected by this. While the latter were generally clean and reliable as expected from these sensors, conductivity measurements sometimes exhibited suspicious values that were potentially caused by particles in the cells. Conductivity values below $20\,\mathrm{mS\,cm^{-1}}$ and above $40\,\mathrm{mS\,cm^{-1}}$ were flagged as "4 — bad"; at time, this coincided with the conductivity issue outlined above. For the five longest time series (∼10 months), a moving average filter was tested and tuned to identify the outliers that still fell within the allowed global range. No suitable window size was found that would exclusively catch the outliers, so we decided to rather flag the remaining suspicious records manually, as "3 — questionable". Further, 2019O3-10m exhibited a small but suspicious, several-day long conductivity drop from 34.1 to 33.5 PSU in June 2020, which was not accompanied by a change in temperature and thereby subsequently flagged as "3 — questionable".

Buoy 2019O6 exhibited more outliers than the other buoy datasets. Since these outliers were not found on the recovered CTDs themselves, we conclude that this was caused by an issue in the inductive modem communication, rather than a problem with the CTD sensor measurement. Since these outliers were too numerous for manual flagging, a moving average filter (window size 14) was applied to determine and flag these records as "3 — questionable" (∼1000 total records for 2019O6). The few remaining outliers (<20) were manually flagged. Interestingly, in some instances this inductive modem issue resulted in records being wrongly assigned; i.e., a measurement taken by 2019O6-10m was assigned by the buoy to 2019O6-20m. In

230 these cases, the records were reassigned and flagged as "2 — modified". 2019O6 temperature and pressure suffered the same problem. The temperature was checked using subsequent moving average filters (window sizes 14 and 11; ∼1900 outliers flagged as "3 — questionable"), and the remaining few outliers were manually flagged as either "3 — questionable" or "2 — modified".

When CTD data was available, the 0.1 dbar and 10 minute resolution buoy pressure records were linearly interpolated in
235 time using the CTD pressure records to achieve a consistent pressure time series. The interpolated records were flagged as "2 — modified" accordingly. For the periods where CTD data was available, this procedure also removed the pressure outliers caused by the inductive modem issue from the 2019O6 record, so no additional filtering was necessary. Each CTD record for a given buoy was assigned a GPS position by linear interpolation of the corresponding buoy GPS record, and drift speed was recalculated accordingly. Instrument depth was calculated from clean pressure readings and latitude using the Matlab GSW
240 toolbox function "gsw_z_from_p", (McDougall and Barker, 2011).

Although practical salinity was initially calculated and provided on the server side, we recalculated this variable from conductivity, temperature, and pressure according to the PSS-78 algorithm (Matlab GSW Toolbox function "gsw_SP_from_C"). Quality flags for calculated depths and salinities were inherited from T, C, and p. Finally, salinity was despiked using a moving average filter with a window size of 12 (equivalent to between 20 and 120 min), depending if the dataset contained 2 min or 10
245 min data. The final (<120) outliers identified by this filter were flagged as "3 - questionable". An overview of the processing and flagging procedure is given in Fig. 2.

4 Results

4.1 Dataset description

The processing described above yielded eight individual time series, one for each buoy. Three time series (2019O2, 2019O7,
250 and 2019O8) only comprise a few weeks, while five (2019O1, 2019O3, 2019O4, 2019O5, and 2019O6) are ∼10 months long. For 2019O1, 2019O3, 2019O4, and 2019O6, we supply a merged product that combines buoy and CTD data, while for 2019O2, 2019O5, 2019O7, and 2019O8, only the transmitted buoy records are available.

The measured oceanographic variables are conductivity, in situ temperature, and pressure, the derived variables are practical salinity and depth. A primary quality flag (1 — good, 2 — modified, 3 — questionable, 4 — bad, 9 — missing data) is given
255 for each of these 5 variables. Each measurement has a corresponding timestamp. Only the buoy measurements (indicated by a "buoy_flag") initially had a GPS record, and a position was given to the higher resolving CTD records by linear interpolation. The drift speed was calculated from the difference between GPS positions. Additionally, the buoy measured surface temperature and a "submerged boolean", which indicates whether the buoy was in seawater or not. Refer to Table 2 for a summary of all variables in each processed dataset. An overview of all individual datasets and the corresponding collections for raw and
260 processed data is given in Table 3.
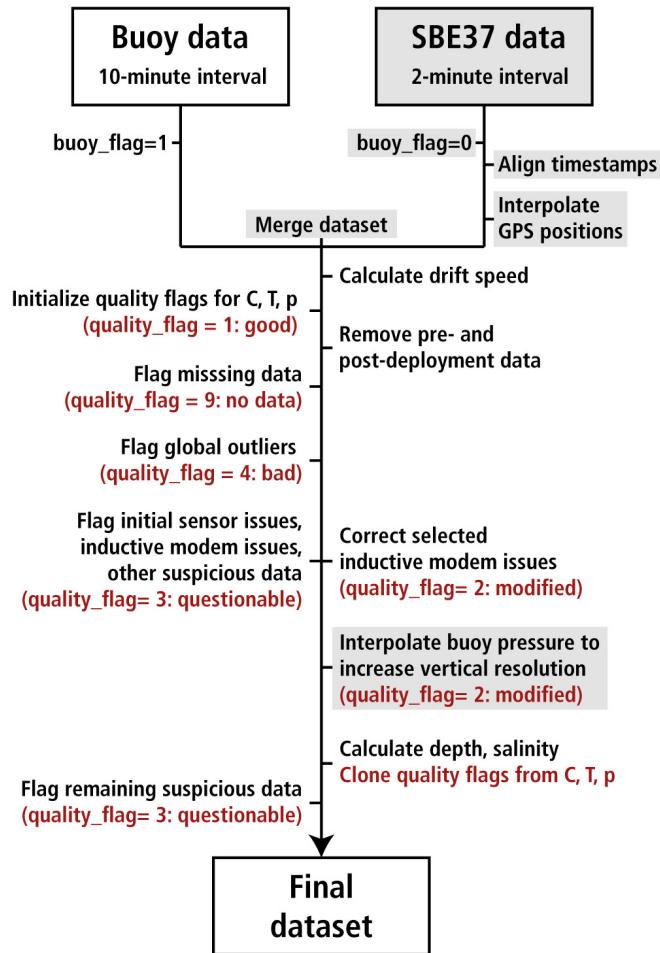
Figure 2. Schematic outlining the individual steps of data processing and quality control using primary flags (indicated in red) according to a slightly modified version of UNESCO-IOC (2013). The additional processing steps required when merging buoy and recovered CTD data are indicated in grey. Procedures to the left of the processing arrow represent flagging without modification of the original data, whereas processing steps to the right involve removal and modification of original data, or calculation of secondary parameters.

Table 2. Variables of the processed dataset. The nominal depths of the 5 CTDs (represented by Gear ID 1-5) were 10m, 20m, 50m, 75m, and 100m. The actual depths are given by the "Depth" variable. * The reduced pressure accuracy accounts for the rounding by the buoy controller before transmission.

Variable	Unit/Format	Accuracy
Date & Time	ISO-8601	1 min
Latitude	deg	
Longitude	deg	30 m
Drift speed	m/s	0.1
Submerged Boolean	logical	
Temperature, surface	°C	0.05 (in water)
Gear ID	1 - 5	
Conductivity, seawater	ms/cm	0.003
Temperature (in situ), seawater	°C	0.002
Pressure, seawater	dbar	0.1 / 0.02*
Depth, instrument	m	0.1 / 0.02*
Salinity, seawater	PSU (PSS-78)	0.01
buoy_flag	logical	
C_flag	1 - good	
T_flag	2 - modified	
p_flag	3 - questionable	
D_flag	4 - bad	
S_flag	9 - missing data	

Table 3. Overview of datasets described in this paper. * indicates datasets that include data from recovered SBE37 CTDs along with the transmitted buoy data. This needs to be updated once accepted.

Level	Buoy ID	Reference	Link
Raw data	2019O1*	Hoppmann et al. (2021a)	https://doi.pangaea.de/10.1594/PANGAEA.933934
	2019O2	Hoppmann et al. (2021b)	https://doi.pangaea.de/10.1594/PANGAEA.933928
	2019O3*	Hoppmann et al. (2021c)	https://doi.pangaea.de/10.1594/PANGAEA.933932
	2019O4*	Hoppmann et al. (2021d)	https://doi.pangaea.de/10.1594/PANGAEA.933933
	2019O5	Hoppmann et al. (2021e)	https://doi.pangaea.de/10.1594/PANGAEA.933937
	2019O6*	Hoppmann et al. (2021f)	https://doi.pangaea.de/10.1594/PANGAEA.933941
	2019O7	Hoppmann et al. (2021g)	https://doi.pangaea.de/10.1594/PANGAEA.933939
	2019O8	Hoppmann et al. (2021h)	https://doi.pangaea.de/10.1594/PANGAEA.933942
Collection	all	Hoppmann et al. (2021i)	https://doi.pangaea.de/10.1594/PANGAEA.937271
Processed data	2019O1*	Hoppmann et al. (2022a)	https://doi.pangaea.de/10.1594/PANGAEA.940271
	2019O2	Hoppmann et al. (2022b)	https://doi.pangaea.de/10.1594/PANGAEA.940298
	2019O3*	Hoppmann et al. (2022c)	https://doi.pangaea.de/10.1594/PANGAEA.940282
	2019O4*	Hoppmann et al. (2022d)	https://doi.pangaea.de/10.1594/PANGAEA.940291
	2019O5	Hoppmann et al. (2022e)	https://doi.pangaea.de/10.1594/PANGAEA.940301
	2019O6*	Hoppmann et al. (2022f)	https://doi.pangaea.de/10.1594/PANGAEA.940296
	2019O7	Hoppmann et al. (2022g)	https://doi.pangaea.de/10.1594/PANGAEA.940303
	2019O8	Hoppmann et al. (2022h)	https://doi.pangaea.de/10.1594/PANGAEA.940304
Collection	all	Hoppmann et al. (2022i)	https://doi.pangaea.de/10.1594/PANGAEA.940320

4.2 Drift trajectories

The drift trajectories of all eight buoys are shown in Figure 3. Their journey alongside the Central Observatory, from the deployment area north of the Laptev Sea through the Transpolar Drift until their recovery in Fram Strait, took about 10 months. The buoys traveled over the Gakkel Ridge from the Amundsen Basin to the Nansen Basin in March/April 2020. The drift accelerated strongly from June onwards upon reaching the Yermak Plateau. While a detailed discussion of the drift pattern is beyond the scope of this paper, it should be noted that the relative positions of the buoys within the array did not change much before finally entering the Fram Strait area (Figure 3).

265
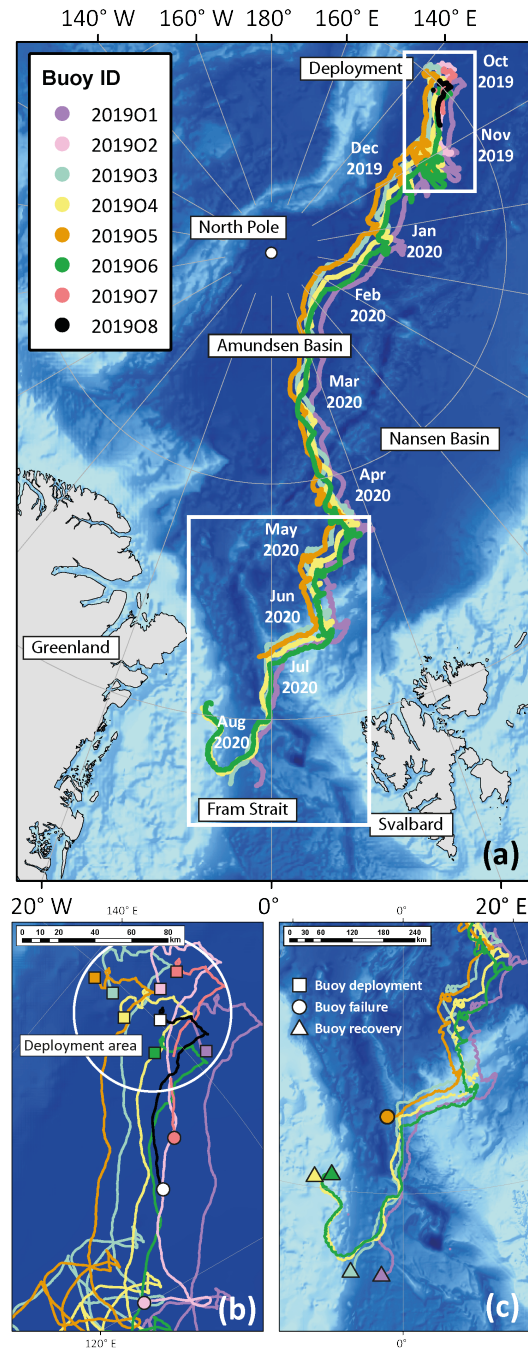
Figure 3. Maps of buoy drift trajectories through the Arctic Transpolar Drift between October 2019 and August 2020. a) Overview map; b) initial setup north of Laptev Sea and first weeks of drift; c) last weeks of drift in Fram Strait. Squares indicate deployment locations, circles indicate locations of failure or recovery. Bathymetric data were obtained from the IBCAO project (Jakobsson et al., 2020). Coastline data is taken from Wessel and Smith (1996).

4.3 Oceanographic data

In the following, we take a closer look at each of the processed datasets shown as time series plots in Figs. 4 and 5. The
corresponding T-S diagrams are provided as a supplement in the Appendix (Fig. A1). As stated earlier, we refer to a specific
instrument time series as "buoy name - nominal instrument depth". For simplicity, we use the buoy name and instrument
references as a synonym for the time series itself.

2019O1 (Fig. 4a) was generally performing well, except for some problems at the beginning of its life cycle. 2019O1-10m
and 2019O1-20m showed a suspiciously low salinity for the first few days after deployment, before adjusting to consistent
levels. 2019O1-75m and 2019O1-100m had the same issue in the very beginning (lasting only a few hours), while it took
2019O1-50m a full 2.5 weeks before plausible salinity data were collected. We assume that these instruments were affected by
ice formation in the conductivity cells, which is a known issue when instruments are submerged while still much colder than
the seawater. We acknowledge however that it is quite unusual that it takes an instrument such a long time to recover even when
installed in seawater at the freezing point, but we don't have a better explanation. After this initial adjustment period, 2019O1
continued to collect reasonable data throughout its operational time. The unit was recovered on 5 August 2020.

2019O2 (Fig. 5a) started fine before all instruments were suddenly lifted by 5 m over one hour during an event on 12
November 2019. They remained in place for one day, before they were lifted again by 8 m in a similar event. The buoy was
lost immediately afterward on 13 November 2019.

2019O3 (Fig. 4b) was fine initially, but 2019O3-50m stopped working after several hours following the deployment, and
never resumed transmitting any data. The other 4 instruments were performing well throughout their operational time. During
an event on 17 February 2020, all remaining CTDs were substantially lifted although there was no particularly strong drift at
that time. 2019O3-10m and 2019O3-20m were even lifted as shallow as the ice base, which is unusual. The only explanation
is that the buoy tether got entangled with the co-deployed D-TOP free floating profiler, which possibly got moved closer to the
SIT as a result of converging pack ice conditions. The sensors returned to their original depths after ~30 min and continued to
measure correctly until the buoy was recovered on 03 August 2020.

2019O4 (Fig. 4c) was fine from the start. Due to an unintentionally high measurement interval of 30 s, 2019O4-75m ran out
of power on 20 April 2020 after a period of intermittent failures starting on 11 January 2020. The buoy and all other CTDs
continued to work well until recovery on 14 August 2020.

2019O5 (Fig. 5b) showed some moderate problems. 2019O5m stopped communicating upon deployment. 2019O5-10m
started to exhibit inductive modem communication issues at the end of October 2019. This began with sporadic missing
measurements in the buoy's transmitted afterward"), which subsequently became more frequent throughout November when
roughly half of the measurements were blanks. In the second half of November, the issue gradually disappeared, with transmis-
sions back to normal on 27 November. From late December 2019 onwards, 2019O5-20m and 2019O5-50m started to exhibit
similar issues, again first sporadic, then almost continuously (roughly half of the measurements affected). Interestingly, this
problem never affected both sensors at the same time, the missing transmissions were always "alternating", and sometimes more
or less periodic. From mid-January onwards, 2019O5-50m recovered from this problem, and transmissions were completely
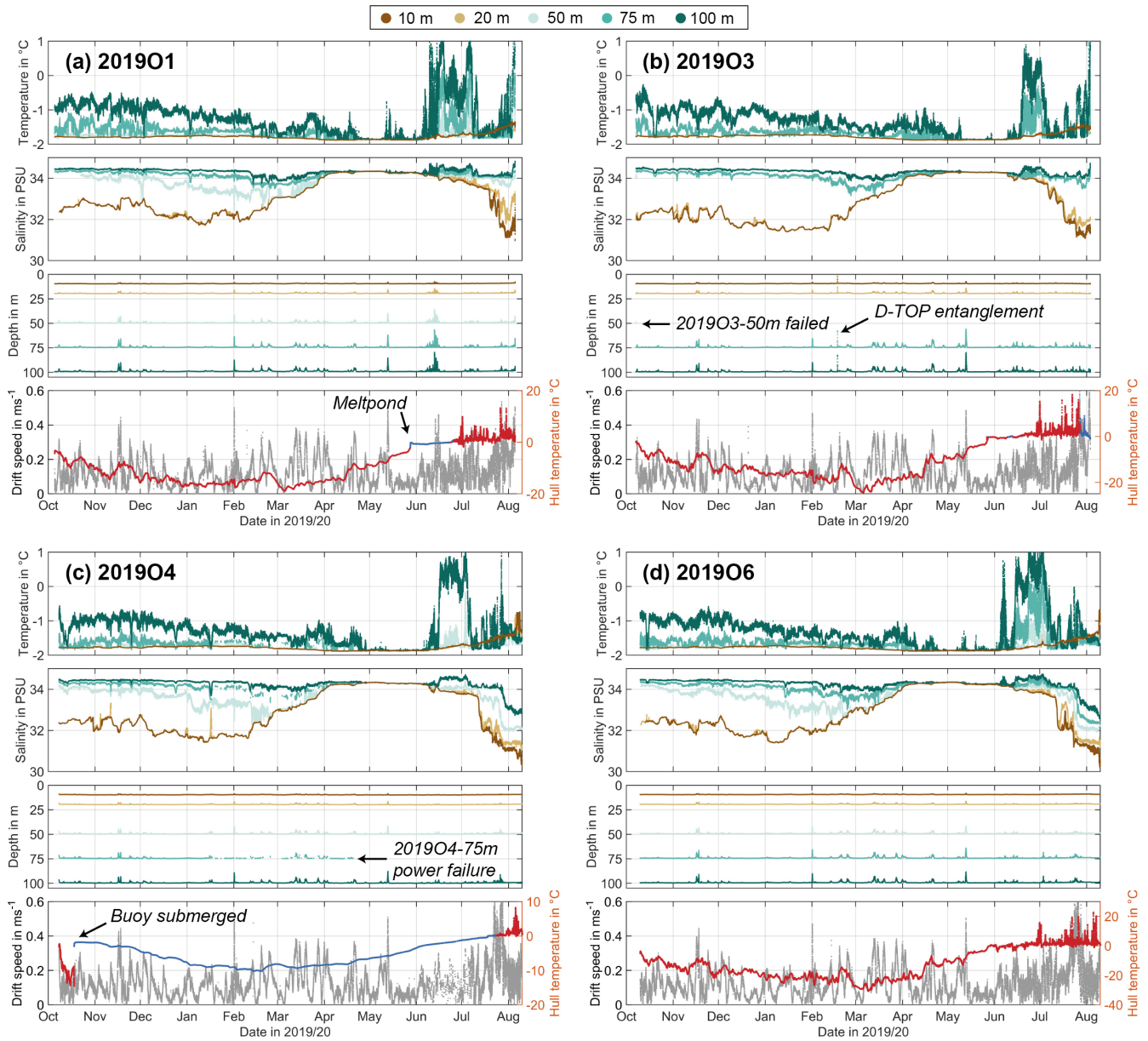
Figure 4. Time series of main variables recorded by buoys and CTDs a) 2019O1; b) 2019O3; c) 2019O4 and d) 2019O6. The panels each show from top to bottom: seawater temperature (ITS-90), seawater practical salinity (PSS-78), instrument depth, buoy drift speed (grey), and surface temperature (blue indicates submerged in seawater, red indicates not submerged). For the oceanographic variables, we only show "1 — good" and "2 — modified" values.
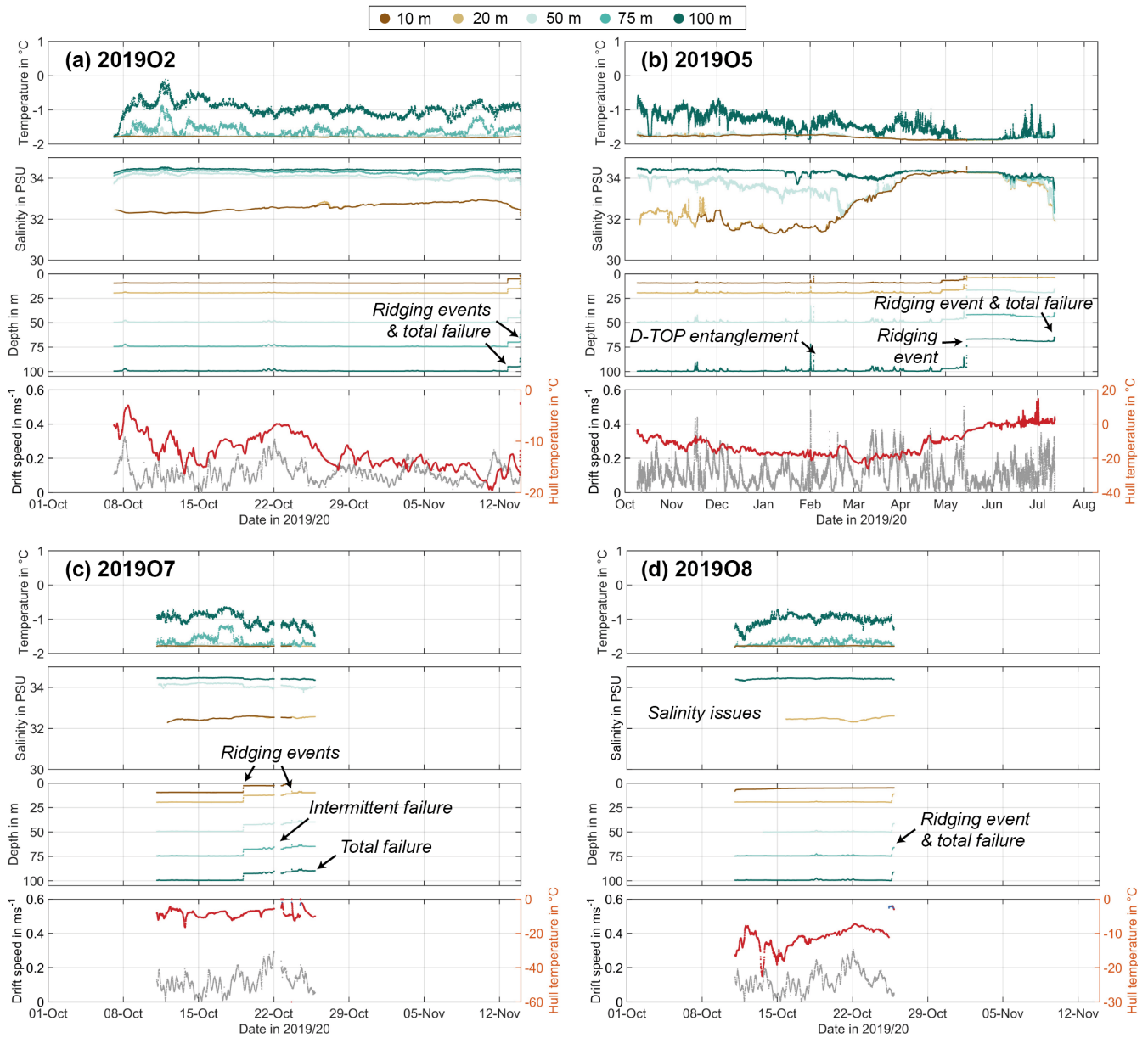
Figure 5. Time series of selected variables recorded by buoys (no recovered CTD data) a) 2019O2; b) 2019O5; c) 2019O7 and d) 2019O8. The panels each show from top to bottom: seawater temperature (ITS-90), seawater practical salinity (PSS-78), instrument depth, buoy drift speed (grey), and surface temperature (blue indicates submerged in seawater, red indicates not submerged). For the oceanographic variables, we only show "1 — good" and "2 — modified" values.

normal from the end of January 2020 onwards. However, the issue with 2019O5-20m persisted until mid-February 2020, with failures still being somewhat periodic at times, when the blanks slowly started to decrease. In late February, the problem with 2019O5-20m was also gone, when 2019O5-100m started to exhibit blanks, with the same pattern: first sporadic, then much more frequently. In late April they became only sporadic again, with a very small fraction of blanks during the remaining buoy lifetime. The reason for this behavior remains unclear. On 14/15 May 2020, a drastic event took place: 2019O5-50m and 2019O5-100m showed a sudden 30 m pressure decrease on that day, suggesting that the entire buoy was lifted by that amount, presumably in a substantial ridging event. Communication to 2019O5-10m was lost in the process, as it was probably torn off the tether. At the same time, however, 2019O5-75m started to transmit data again, at a current depth of ∼45 m (as expected as the event lifted the instrument from a nominal depth of 75 m). 2019O5-20m was only lifted by 16 m, to a depth of 4 m, suggesting that it was pushed down along the tether by the resistance of the ice bottom. Surprisingly, the sensor survived this incident. The buoy kept collecting reasonable data via the four remaining CTDs (2019O5-20m presumably directly from the ice base), and interestingly without any further inductive modem issues. There were two more events, on 13 and 16 June 2020, during which three of the four instruments suddenly moved down 1 m each, interestingly except for 2019O5-20m, which was then at 3.8 m and presumably somehow stuck in the ice. Another event during which the buoy was lifted by 4 m occurred on 12 July 2020, briefly before the buoy stopped transmitting any more data.

2019O6 (Fig. 4d) was generally performing well but suffered from an issue with the inductive modem link between the buoy and the CTDs. 2019O6-10m had some minor conductivity cell issues in the first few days after deployment. The buoy started to suffer from inductive modem communication issues with all instruments on the tether, which became worse from November 2019 onwards but significantly improved again from 13 April 2020 for unknown reasons. These issues resulted in erroneous values being recorded by the buoy (in contrast to the problems with 2019O5, where measurements were just blank), leading to a large number of outliers in the raw dataset. On 03 August 2020, all CTDs exhibited a sudden increase in pressure of 0.5 dbar, probably related to a draining melt pond (although the submergence sensor was never triggered) or a similar effect that caused the surface buoy to slightly drop. The unit was recovered on 13 August 2020.

Similar to 2019O2, buoys 2019O7 and 2019O8 (Fig. 5c,d) were also fairly short-lived. 2019O7-75m suffered from conductivity cell issues upon deployment and did not recover. All instruments were lifted by 7 m during an event on 19 October 2019. The instruments were at stable depths for a few days, before they were lifted again over a few days between 22 and 24 October. 2019O7-10m was lost eventually, and the buoy stopped transmitting entirely on 26 October 2019. Three instruments on 2019O8 had issues with ice in the conductivity cell upon deployment, which lasted until the end of its (short) operational time. On 25 October 2019, all instruments were lifted by 10m over a few hours, with 2019O8-10m being stuck at the ice bottom and pushed down the tether. A few hours after that, the buoy stopped transmitting.

5 Discussion

In this section, we assess the quality of the oceanographic data and discuss the general instrument performance. We showcase the strength of the deployment concept and potential of the dataset as a whole and discuss the wider role of the data, in particular, the potential within the framework of MOSAiC.

5.1 Data quality & validation

In addition to a general data plausibility and consistency check among individual (independent) CTDs installed on the same tether as performed during the data processing, there are a few other methods to assess the general data reliability and quality. These will be elaborated on in this section.

5.1.1 Post-deployment calibration

The CTDs were manufactured and laboratory-calibrated by Seabird only 2 months before deployment. Post-deployment calibration was performed at Seabird for three sets of CTDs (2019O3, 2019O4, 2019O6; 15 in total) in July 2021. 2019O1 was re-deployed during the final MOSAiC leg a few weeks later as 2020O10 (not shown here), so the five corresponding CTDs were not available for post-deployment calibration. We decided to not apply any correction to the temperature and salinity data based on this calibration information (see below). Further, the schedule of our logistics operations and onboard tasks did not allow us to conduct in situ calibration for each CTD using the higher-accuracy ship-based Seabird SBE911+ system. However, there was the possibility of cross-validation to concurrent observations taken nearby during visits to the sites (see Section 5.1.2).

The results of the post-deployment calibration were within normal limits for this instrument type (Table 4). While a temperature offset and conductivity drift correction of the data according to Seabird's Application Note 31 was considered, we decided not to apply this procedure to the present data set for the following reasons: the offset in temperature (usually mainly by electronic drift) was generally on the order of $\pm 0.0005°C$, which is within the noise level of the instruments. In addition, the calibration sheets show that the main contribution to the calculated offset stemmed from bath temperatures $>5°C$, which is much higher than ambient temperatures for the upper 100 m of the water column. The conductivity drift, which is usually mainly a result of fouling processes within the conductivity cell, was also generally low. The problem with fouling is that the usual assumption of a linear change is not necessarily true. Such a change can also occur suddenly, and the calibration does not account for the timing. Assuming the fouling would lead to a linear drift of the cell, the instrument is treated in various ways and exposed to different environmental conditions between the recovery and the actual calibration. It is usually cleaned, packed, transported, and stored, so the calibration results are not necessarily reflecting the conditions under which the instrument took the measurements. Finally, an open question is whether to perform the linear correction between the calibration dates (as recommended by Seabird), or between deployment and recovery, where fouling can occur. Due to the issues we described with possible calibration of the instruments we decided to not correct the values measured by each sensor and, instead, validate the measurements to estimate how reliable they are. The results from our calibration procedure suggest that all instruments in

Table 4. Temperature offset and conductivity drift from post-deployment calibration. Pressure (not shown) did not drift at all. This information is provided here for reference. Corrections have not been applied to the data (see text).

Buoy	Depth	SN	pre-cal	post-cal	C-slope	T-offset in mdeg
2019O3	10	21100	18-Aug-2019	13-Jul-2021	0.9999781	0.44
	20	21103	18-Aug-2019	09-Jul-2021	1.0002158	-0.06
	50	21113		mainboard broken		
	75	21114	16-Aug-2019	08-Jul-2021	0.9996651	0.57
	100	21084	12-Aug-2019	15-Jul-2021	0.9999438	-0.19
2019O4	10	21093	18-Aug-2019	13-Jul-2021	0.9995212	0.35
	20	21094	18-Aug-2019	09-Jul-2021	0.9999413	0.07
	50	21095	14-Aug-2019	13-Jul-2021	1.000185	0.39
	75	21099	25-Aug-2019	13-Jul-2021	1.0002775	0.6
	100	21083	12-Aug-2019	27-Jul-2021	0.999825	0.15
2019O6	10	21112	19-Aug-2019	08-Jul-2021	0.9999426	0.29
	20	21115	18-Aug-2019	13-Jul-2021	1.0001306	0.21
	50	21116	18-Aug-2019	13-Jul-2021	1.0001337	0.4
	75	21117	18-Aug-2019	13-Jul-2021	1.0000979	0.69
	100	21108	19-Aug-2019	13-Jul-2021	1.0005926	-0.69

Table 4 can be considered reliable. As a final note, 2019O3-50m was diagnosed with a mainboard failure and was replaced on warranty.

5.1.2 Validation using independent measurements

A wealth of hydrographic data was collected during MOSAiC at different times and places as part of the physical oceanography program. Specifically intended to validate the buoy data in situ, several deployment sites were revisited during April and May 2020. Several water column profiles were obtained using two handheld unpumped, self-recording CTDs (SST48M, Sea&Sun Technologies, Germany; hereafter referred to as "SST-CTD"). The instrument was mounted on the line of a fishing rod with a battery-powered winch to measure profiles of temperature, salinity, and pressure in the upper water column. A total of 5 SST-CTD profiles were taken at different deployment sites (see table A1).

In addition to the manufacturer's calibration, the two SST-CTDs were mounted on a standard ship-based high-accuracy CTD-Rosette system for in situ calibration (Seabird SBE911+, hereafter referred to as "ship CTD" for simplicity) to validate
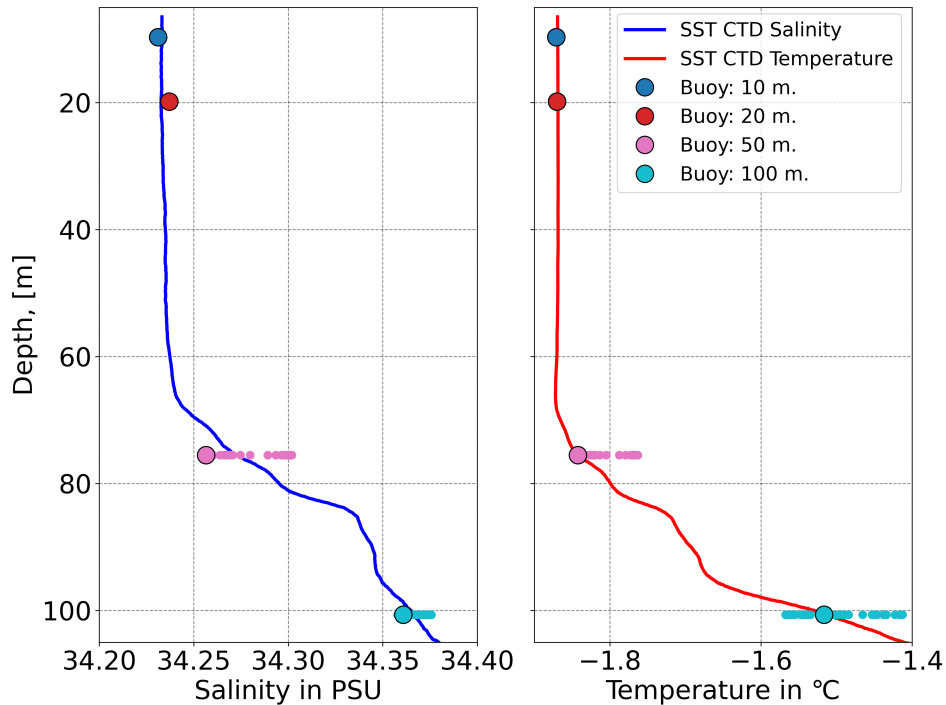
Figure 6. Comparison between SST-CTD and 2019O3 data on 26 April 2020. Red and blue lines represent salinity and temperature recorded by the SST-CTD, respectively. Circles represent buoy data closest in time to the SST-CTD cast. The colored dots show the values of the corresponding buoy CTD within half an hour before and after the SST-CTD cast. Buoy data at 10 and 20 m are hidden below the circles.

375   the sensors themselves. These inter-calibration exercises were carried out in February and July 2020, close in time to the validation casts at the buoy sites to minimize the potential influence of unaccounted sensor drift. The results of these calibration casts showed a deviation of both SST-CTD's pressure from the ship CTD of approximately 1 m at 100 m depth. This has been taken into account for the comparison to the buoy data by smoothing the profile. SST-CTD salinity and temperature deviations were largest within the halocline and upper permanent pycnocline (e.g. Polyakov et al., 2013), as can be expected for these

380   kinds of inter-calibration experiments. The average salinity and temperature offsets were 0.008 PSU and 0.006°C, respectively, and have been corrected. For comparison with the buoy data, the SST-CTD validation profiles have been smoothed using a Savitzky-Golay filter (window size of 31, corresponding to about 3.5 m). An example of the comparison is shown in Figure 6. The average deviation values between SST-CTD and the buoy temperature and salinity are δT=-0.002$\pm$0.002°C and δS=-0.004$\pm$0.006 PSU, respectively, which is within the stated accuracy of the SST-CTD sensors (given by the manufacturer

385   as 0.002°C for T and 0.002 ms cm^{-1} for C). In conclusion, the CTDs on the buoys show very good agreement with the intercalibrated SST-CTDs after a measurement period of 6 months.

5.1.3 Data transfer issues

An additional source of error that is not necessarily obvious is introduced by quirks in the inductive modem communication between the instruments and the surface package of the buoy. The reliability of the oceanographic data polled from the individual CTDs by the surface electronics via the inductive modem link can be assessed by comparison of the buoy data set to the data collected internally by the 20 individual CTDs that were recovered in August 2020. This comparison confirmed that the buoys generally operated as intended. However, in the case of 2019O6, this comparison helped to identify and remove a large number of outliers that seemingly resulted from an (unknown) issue in the inductive modem communication.

The transmission of data via iridium (in this case the short burst data protocol) may be sometimes unstable due to a variety of reasons, but usually only leads to the unit not being able to transfer a data package in the first place, or more rarely, to the loss of individual data packages. This technique generally does not introduce errors in the recorded data itself as far as we are aware.

5.2 Properties of an observed eddy

Here we present a prominent example of the type of features observable with the present instrumentation and overall approach: a mesoscale eddy that passed through the buoy array in February 2020. During that time, the MOSAiC observatory drifted towards the northwest at an average velocity of about $0.13 \ \mathrm{ms^{-1}}$. The number of loops was considerably less compared to the previous November and December (Fig. 7a). The buoys drifted along a pronounced surface salinity gradient, from less saline water in the southeast to more saline in the northwest (Fig. 7). The lateral gradients of salinity and temperature are evident from both, the time series along each buoy track, as well as in the observations between different buoys.

Although our measurements are confined to discrete depths, the CTD records at 20 and 50 m can still indicate the minimum mixed-layer depth if they show equal temperature and salinity. Thereby, we infer from the records of 2019O4 and 2019O6 that the depth of the upper ocean mixed layer (ML) increased to >50 m from about mid-February onwards. This is in agreement with less frequent observations by an ocean profiler (Rabe et al., 2022).

Changes in water properties with time at 20 and 100 m depths are shown in the temperature-salinity diagram in Figure 7b. The mixed-layer salinity increased with a corresponding decrease in temperature along the freezing line during February. At the same time, salinity and temperature at 100 m decreased. An increase in mixed-layer salinity could be partly explained by a combination of upward mixing of deep salty water from below and salt rejection during ice formation from above, both forced by two February storms with wind speeds up to 16 m s^{-1} and surface air temperatures of around -15°C. However, close-by near-daily measurements of the vertical mixing properties with a dedicated microstructure probe at the central observatory did not show significant mixing underneath the halocline (K. Schulz, pers. comm.). Further mixed-layer deepening occurred into early April (Fig. 4) when the ML depth reached 100 m. Between February and April, the drift path of the buoys was about 340 km, or 270 km straight line distance. They drifted across the front associated with the transition from the Transpolar Drift to the warm and salty inflow of water of Atlantic origin through the Fram Strait. These types of upper ocean salinity gradients generally provide a high potential to form eddies.
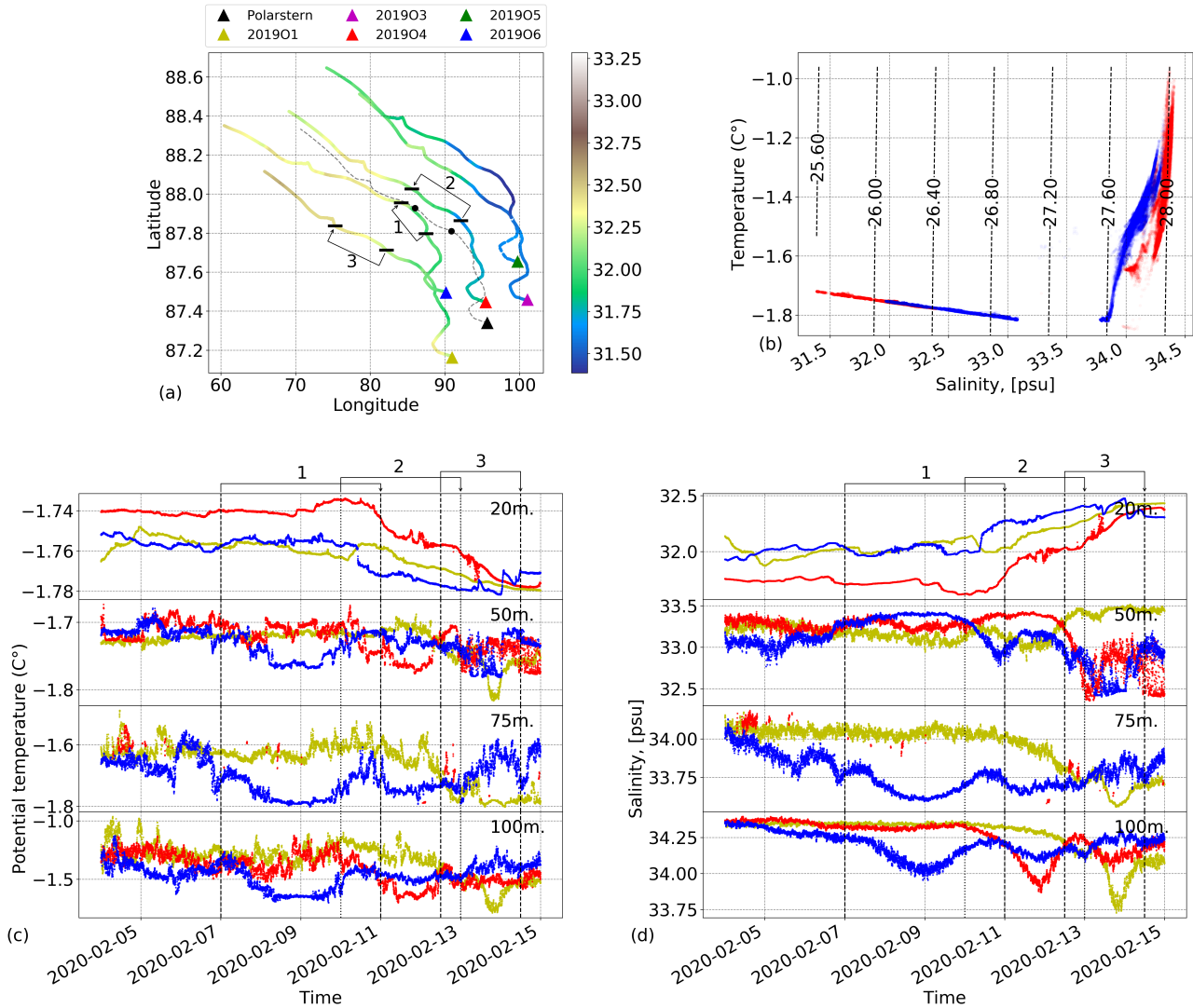
Figure 7. Preliminary observations of an eddy passing through the Distributed Network in February 2020. a) Trajectories and observed salinity at 10 m depth of 5 buoys (colored) along with trajectory of RV *Polarstern* (black) between 02 and 20 February 2020. Triangles indicate the buoy positions on 02 February. The black horizontal lines with numbered bars indicate the start and end positions of the times in c and d, where changing water properties were observed by the corresponding buoy. b) T-S diagram of buoy data at 20 and 100 m depth during 01 to 20 February 2020 (red) and 20 February to 01 March 2020 (blue). c) and d) Temperature and salinity recorded at four different depths by buoys 2019O1, 2019O4, and 2019O6. The line colors correspond to the triangle colors in a.

During 7 - 10 February, rapid changes in the water properties were registered by 2019O4, 2019O6, and, to a lesser extent, 2019O1. 2019O6 (blue triangle and lines) and 2019O4 (red triangle and lines) registered these changes four and one days in advance of *Polarstern* reaching the same location, respectively. The evolution of the observed salinity values showed a tendency for saltier waters appearing at depths shallower than $\sim$50 m and fresher waters deeper than 70 m. For example, the salinity decreased by 0.22 and 0.17 at 100 and 75 m, respectively, and increased by 0.5 at 50 m depth for buoy 2019O6. Temperature evolution was less conclusive since most measurements were within the range of the cold halocline layer. This feature indicated the presence of an eddy with approximate geographical locations registered by the buoys as shown by two short lines (beginning and end) on the buoy tracks (Fig. 7a) and colored shaded areas in Figure 7c,d with buoy temperatures and salinities at four depths, 20, 50, 75 and 100 m. The CTDs at 10 m depth show mostly the same water properties as those at 20 m. Line colors correspond to the triangle colors of the buoys in Figure 7a. This event was also observed by the current measurements obtained by the shipboard Acoustic Doppler Current Profiler (ADCP). It showed the presence of the eddy between 11 and 13 February (S. Tippenhauer, pers. comm.), and the location is denoted in Figure 7a (black dots on the dashed line). Most likely, the ship drifted close to the center of the eddy. It exhibited a rather symmetric current structure, with the minimum speed in the center and currents on the sides in opposite directions with speeds up to 20 m s^{-1}. The estimated diameter of the eddy based on the buoy drift was about 30 km. A detailed description of the eddy properties is beyond the scope of this paper and is the subject of ongoing work.

It is important to note that the drift speed increased from 0.04 to 0.2 m s^{-1} between 07 and 14 February. Thereby, the time interval when the eddy was observed by different buoys decreased while the drifting distance (or eddy diameter) remained similar. At the same time, 2019O3 and 2019O5 did not show significant changes at a depth of 100 m. Both buoys were located to the northeast of the ship. Likely, they were too far away from the core of the eddy to register a measurable signal.

All three buoys that registered the eddy encountered similar anomalies in temperature and salinity. The salinity decreased by 0.22 and 0.17 at 100 and 75 m, respectively, and increased by 0.5 at 50 m depth with a corresponding temperature decrease of 0.3, 0.12 and 0.05°C for buoy 2019O6. We also calculated the bulk buoyancy frequency, $N^2 = -\frac{g}{\rho_0}\frac{d\rho(z)}{dz}$, using measurements between 50 and 100 m. The result shows that N decreased during the passing of the eddy from $\sim$8 to 5.7 cph for 2019O6, from $\sim$7.2 to 5.1 cph for 201904, and from $\sim$6 to 4 cph for 201901. If we use the simplest way to calculate the first mode baroclinic Rossby radius, using $L_R \equiv \frac{NH}{\pi f_0}$ with a constant $N = 5$ cph and $H = 4500$ m, L_R is around 14 km (corresponding to a diameter of 28 km), and close to the estimated diameter of the eddy. The distributed nature of the buoys allowed a fully synoptic assessment at different points across the array, which could not have been achieved by just one buoy.

5.3 Wider scope of the dataset

The example in Section 5.2 shows how our data can be used to study mesoscale features in the upper Arctic Ocean. The wider scope of science questions that could be studied with the data is broad: the seasonality could be explored further, as well as the variability along the pathways of the TPD (e.g. Stedmon et al., 2021). In particular, the buoy data fills the winter gap common to manual in-situ observations, that are often carried out during seasonally limited ship surveys. The high temporal resolution allows for studying passing transient and submesoscale phenomena, as the buoys acted as a quasi-
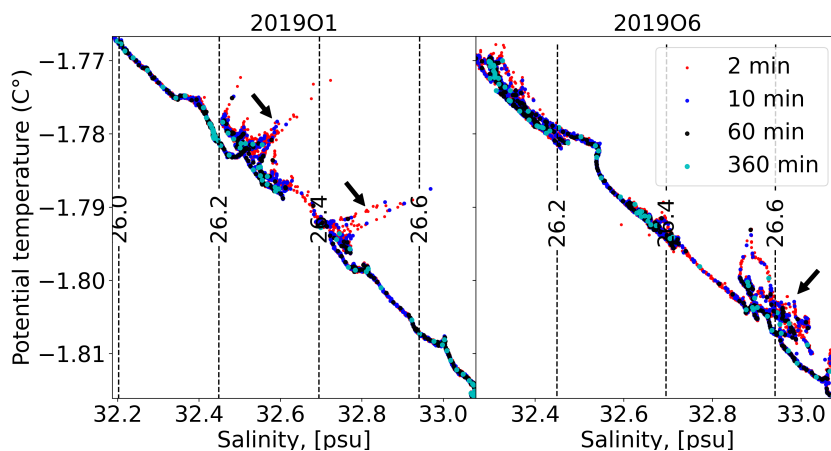
Figure 8. T-S diagram of observations during 12 February – 1 March 2020, at 20 m from (a) 2019O1 and (b) 2019O6. Dots with different colors denote different temporal resolutions. Black arrows highlight features that can be only resolved with high-resolution data.

stationary platform, depending on drift speed. On the other hand, during times of faster drift, the systems measured the upper
455 ocean quasi-synoptically over submesoscales.

This allows us to observe small-scale spatiotemporal variability of temperature and salinity that may be overlooked by traditional platforms. Measurements along a fixed isobath on a scale of hours correspond to a spatial resolution of ~ 10 km (e.g, like those collected from ships or Ice-Tethered Profilers) and normally resolve mesoscale features. This may be illustrated by subsampling our buoy data at an interval of 60 and 360 min (Figure 8), revealing a near-surface frontal structure in the T-S
460 diagram with warmer (colder) and fresher (saltier) at either side of the front. Note that the nominal capacity of our buoys allows <10 min ($<\sim 1$ km) resolution data, thus the buoys further capture phenomena hidden in this frontal structure. For example, there appears to be a density compensation process with warmer, saline waters compensating those with lower temperature and salinity (see black arrows in Figure 8a). Another nearby buoy sees the same large-scale front but may additionally observes a local thermohaline intrusion within the front (see black arrow in Figure 8b).

465 The significance of submesoscale circulation has been shown in numerous studies, highlighting the associated strong vertical velocity (Biddle and Swart, 2020; Mahadevan et al., 2010), restratification processes (Timmermans et al., 2012; du Plessis et al., 2019), conversion of potential to eddy kinetic energy (Zhang et al., 2019) and feedback between ice and ocean currents around filaments in the marginal ice zone (MIZ) (von Appen et al., 2018). These physical processes can significantly influence bio-geochemical conditions and the ecosystem (Fadeev et al., 2021; Kaiser et al., 2021). Yet, the submesoscale is largely limited
470 to regional models or idealized process simulations (e.g. Manucharyan and Timmermans, 2013; Manucharyan and Thompson, 2017), and largely out of reach for state-of-the-art numerical ocean general circulation models, necessitating appropriate parameterizations (Lévy et al., 2012, e.g.).

Analyzing our dataset further could make use of horizontal wavenumber spectra, that can give insights into the length scales of variability induced by submesoscale restratification and internal waves (Marcinko et al., 2015; Timmermans et al., 2012). Furthermore, submesoscale eddies and filaments between mesoscale features can be studied with this piecewise quasi-synoptic dataset.

The scientific results of these potential studies, as well as the data itself, could serve to validate numerical models of the ice-ocean system and the fully coupled earth system. The observations can also serve as input to numerical models, either to initialize or force a simulation or to provide input for assimilation. Finally, the GPS data recorded by our buoys were also used to create the "official" drift trajectories for several of the main sites of the Distributed Network (Nicolaus et al., 2021b).

6 Conclusions & Outlook

We have shown results from a unique deployment of several ice-tethered buoy systems measuring temperature and salinity in the upper 100 m of the central Arctic Ocean. These systems were part of the MOSAiC expedition, a year-long drift of the German icebreaker RV *Polarstern* in 2019/20. The deployment concept was specifically designed to observe mesoscale and, to a lesser degree, submesoscale variability, including internal waves, in the ocean mixed-layer and upper halocline throughout different seasons and across the Eurasian Basin. Additionally, the buoys provided valuable oceanographic data as a complement to various other co-located multidisciplinary ice-tethered buoy systems and the overall MOSAiC work program. The buoy systems generally performed well, with a few expected failures due to ice deformation, in particular, as the sea ice environment was even more dynamic than anticipated. An added value was obtained by recovering four of the eight buoys, yielding data at an even higher temporal resolution. We have shown through a validation approach that the temperature and salinity measurements by our buoy systems are accurate, and capable of showing details of an upper ocean eddy during the Arctic winter. Additionally, post-deployment calibration only showed minor sensor drift. The dataset is expected to be of significant value for example for future process studies, even beyond MOSAiC, and for the validation of numerical models aimed to better understand the role of the crucially important though barely studied Arctic Ocean in the Earth's climate system.

On a final note, buoy 2019O1 was redeployed in the new ice camp of MOSAiC Leg 5 close to the North Pole in August 2020 as 2020O10. As of August 2022, this buoy has reached Iceland, although the CTDs ran out of power a few months earlier. Since this deployment was not part of the array, we decided to not include it in this paper. However, we will apply a similar processing to this dataset for consistency, as well as to future deployments of similar buoys that are already planned for 2022, 2023, and 2024.

7 Code and data availability

Collections of the presented raw and processed datasets are available under https://doi.pangaea.de/10.1594/PANGAEA.937271 (Hoppmann et al., 2021i) and https://doi.pangaea.de/10.1594/PANGAEA.940320 (Hoppmann et al., 2022i), respectively (both currently under moratorium). An overview of all individual raw datasets (including unprocessed buoy- and CTD data), as well

as all fully processed and quality-controlled datasets, is given in Table 3). A token for temporary access to the reviewers can be generated at https://www.pangaea.de/tok/147f801ef2a96849e4c64c1fd3eedf31aa802c21 for the processed data and https://www.pangaea.de/tok/88bfe8f850838ba2de6da30302f9079a35723e63 for the raw data. The Matlab code used to create the processed dataset is available on request. This needs to be updated once accepted.

Author contributions. BR was responsible for the initial conceptualization of the study. The methodology was proposed by BR, and further enhanced by MH, YCF, and IK. BR and MH were responsible for the project administration. MH and YCF deployed the instruments in the field. MH was responsible for data curation, prepared the original draft, and visualized the data. IK conducted the data validation and eddy studies. All authors contributed to the review and editing of the manuscript.

Competing interests. There are no competing interests associated with this study.

Acknowledgements. Data presented in this paper were produced as part of the international Multidisciplinary drifting Observatory for the Study of the Arctic Climate (MOSAiC) with the tag MOSAiC20192020 (grant numbers AWI_PS122_00 and AFMOSAiC-1_00). We thank Andy Sybrandy and Pacific Gyre for building the buoys. The study was partly funded through the PACES II (Polar regions And Coasts in the changing Earth System) programme and the FRAM (FRontiers in Arctic marine Monitoring) strategic investment by the Helmholtz Association. The instruments were funded as part of the MIDO (Multidisciplinary Ice-based Drifting Observatory) infrastructure. The study contributes to the Changing Arctic Ocean (CAO) program, jointly funded by the UKRI Natural Environment Research Council (NERC) and the BMBF, project Advective Pathways of nutrients and key Ecological substances in the ARctic (APEAR) grants NE/R012865/1, NE/R012865/2 and #03V01461; the project EPICA in the research theme MARE:N - Polarforschung/MOSAiC funded by the German Federal Ministry for Education and Research with funding number 03F0889A; and the European Commission for EU H2020 grant no. 101003472 (project Arctic PASSION). We thank the crews of the research vessels Akademik Fedorov, Akademik Tryoshnikov, and RV *Polarstern*, as well as the helicopter company Naryan-Marsky for their great logistical support that made this study possible. We explicitly like to thank Kathrin Riemann-Campe and Marcel Nicolaus for their help with the intermediate data provision via meereisportal.de, and Wilken-Jon von Appen for his input on the introduction. We express our gratitude to all participants of these expeditions, particularly to the MOSAiC School for their field assistance during the set-up, to Janin Schaffer and the Leg 3 team for their effort to collect the validation data, and to Matthew Shupe, Julia Regnery, Kirstin Schulz and the entire Leg 4 Team for the recovery of the instruments. Full acknowledgments are available in Nixdorf et al. (2021). Finally, we thank the three anonymous reviewers and the editor, Giuseppe M.R. Manzella, for their valuable comments which significantly improved the quality of this paper.

References

Athanase, M., Sennéchael, N., Garric, G., Koenig, Z., Boles, E., and Provost, C.: New Hydrographic Measurements of the Upper Arctic Western Eurasian Basin in 2017 Reveal Fresher Mixed Layer and Shallower Warm Layer Than 2005–2012 Climatology, Journal of Geophysical Research: Oceans, 124, 1091–1114, https://doi.org/10.1029/2018JC0147010, 2019.

Beszczynska-Möller, A., Fahrbach, E., Schauer, U., and Hansen, E.: Variability in Atlantic water temperature and transport at the entrance to the Arctic Ocean, 1997-2010, ICES Journal of Marine Science, https://doi.org/10.1093/icesjms/fss056, 2012.

Biddle, L. C. and Swart, S.: The Observed Seasonal Cycle of Submesoscale Processes in the Antarctic Marginal Ice Zone, Journal of Geophysical Research: Oceans, 125, https://doi.org/10.1029/2019JC015587, 2020.

Bretherton, F. P., Davis, R. E., and Fandry, C. B.: A technique for objective analysis and design of oceanographic experiments applied to MODE-73, Deep Sea Research and Oceanographic Abstracts, 23, 559–582, https://doi.org/http://dx.doi.org/10.1016/0011-7471(76)90001-2, 1976.

Capet, X., McWilliams, J. C., Molemaker, M. J., and Shchepetkin, A. F.: Mesoscale to submesoscale transition in the California Current system. Part I: Flow structure, eddy flux, and observational tests, Journal of Physical Oceanography, 38, 29–43, https://doi.org/10.1175/2007JPO3671.1, 2008.

Chelton, D. B., DeSzoeke, R. A., Schlax, M. G., El Naggar, K., and Siwertz, N.: Geographical Variability of the First Baroclinic Rossby Radius of Deformation, Journal of Physical Oceanography, 28, 433–460, https://doi.org/10.1175/1520-0485(1998)028<0433:GVOTFB>2.0.CO;2, 1998.

D'Asaro, E., Lee, C., Rainville, L., Harcourt, R., and Thomas, L.: Enhanced Turbulence and Energy Dissipation at Ocean Fronts, Science, 332, 318 LP – 322, https://doi.org/10.1126/science.1201515, 2011.

D'Asaro, E. A.: Observations of small eddies in the Beaufort Sea, Journal of Geophysical Research: Oceans, 93, 6669–6684, https://doi.org/10.1029/JC093iC06p06669, 1988.

du Plessis, M., Swart, S., Ansorge, I. J., Mahadevan, A., and Thompson, A. F.: Southern Ocean Seasonal Restratification Delayed by Submesoscale Wind–Front Interactions, Journal of Physical Oceanography, 49, 1035–1053, https://doi.org/10.1175/JPO-D-18-0136.1, 2019.

Fadeev, E., Wietz, M., von Appen, W.-J., Iversen, M. H., Nöthig, E.-M., Engel, A., Grosse, J., Graeve, M., and Boetius, A.: Submesoscale physicochemical dynamics directly shape bacterioplankton community structure in space and time, Limnology and Oceanography, 66, 2901–2913, https://doi.org/10.1002/lno.11799, 2021.

Ferrari, R. and Wunsch, C.: Ocean Circulation Kinetic Energy: Reservoirs, Sources, and Sinks, Annual Review of Fluid Mechanics, 41, 253–282, https://doi.org/10.1146/annurev.fluid.40.111406.102139, 2008.

Gallaher, S. G., Stanton, T. P., Shaw, W. J., Cole, S. T., Toole, J. M., Wilkinson, J. P., Maksym, T., and Hwang, B.: Evolution of a Canada Basin ice-ocean boundary layer and mixed layer across a developing thermodynamically forced marginal ice zone, Journal of Geophysical Research: Oceans, 121, 6223–6250, https://doi.org/10.1002/2016JC011778, 2016.

Gaube, P., Chelton, D. B., Samelson, R. M., Schlax, M. G., and O'Neill, L. W.: Satellite observations of mesoscale eddy-induced Ekman pumping, Journal of Physical Oceanography, 45, 104–132, https://doi.org/10.1175/JPO-D-14-0032.1, 2015.

Gill, A., Green, J., and Simmons, A.: Energy partition in the large-scale ocean circulation and the production of mid-ocean eddies, https://doi.org/10.1016/0011-7471(74)90010-2, 1974.

Gommenginger, C., Chapron, B., Hogg, A., Buckingham, C., Fox-Kemper, B., Eriksson, L., Soulat, F., Ubelmann, C., Ocampo-Torres, F., Nardelli, B. B., Griffin, D., Lopez-Dekker, P., Knudsen, P., Andersen, O., Stenseng, L., Stapleton, N., Perrie, W., Violante-Carvalho, N.,

Schulz-Stellenfleth, J., Woolf, D., Isern-Fontanet, J., Ardhuin, F., Klein, P., Mouche, A., Pascual, A., Capet, X., Hauser, D., Stoffelen, A., Morrow, R., Aouf, L., Breivik, O., Fu, L.-L., Johannessen, J. A., Aksenov, Y., Bricheno, L., Hirschi, J., Martin, A. C. H., Martin, A. P., Nurser, G., Polton, J., Wolf, J., Johnsen, H., Soloviev, A., Jacobs, G. A., Collard, F., Groom, S., Kudryavtsev, V., Wilkin, J., Navarro,

570   V., Babanin, A., Martin, M., Siddorn, J., Saulter, A., Rippeth, T., Emery, B., Maximenko, N., Romeiser, R., Graber, H., Azcarate, A. A., Hughes, C. W., Vandemark, D., Silva, J. d., Leeuwen, P. J. V., Naveira-Garabato, A., Gemmrich, J., Mahadevan, A., Marquez, J., Munro, Y., Doody, S., and Burbidge, G.: SEASTAR: A Mission to Study Ocean Submesoscale Dynamics and Small-Scale Atmosphere-Ocean Processes in Coastal, Shelf and Polar Seas, Frontiers in Marine Science, 6, https://doi.org/10.3389/fmars.2019.00457, 2019.

Hatakeyama, K., Hosono, M., Shimada, K., Kikuchi, T., and Nishino, S.: JAMSTEC Compact Arctic Drifter (J-CAD): A new Generation

575   drifting buoy to observe the Arctic Ocean, Journal of the Japan Society for Marine Surveys and Technology, 13, 1_55–1_68, https://ui.adsabs.harvard.edu/abs/2012JJSMS..13.1.55H, 2012.

Hewitt, C. D., Golding, N., Zhang, P., Dunbar, T., Bett, P. E., Camp, J., Mitchell, T. D., and Pope, E.: The Process and Benefits of Developing Prototype Climate Services—Examples in China, Journal of Meteorological Research, 34, https://doi.org/10.1007/s13351-020-0042-6, 2020.

580   Hill, V., Light, B., and Steele, M.: Collaborative Research: The WArming and irRadiance Measurement (WARM) buoy: Assessing the role of solar energy in heating, photosynthesis, and photo-oxidation in the upper Arctic, 2017-2018, Arctic Data Center, 2019.

Hoppmann, M., Kuznetsov, I., Fang, Y.-C., and Rabe, B.: Raw seawater temperature, conductivity and salinity obtained at different depths by CTD buoy 2019O1 as part of the MOSAiC Distributed Network, https://doi.org/10.1594/PANGAEA.933934, 2021a.

Hoppmann, M., Kuznetsov, I., Fang, Y.-C., and Rabe, B.: Raw seawater temperature, conductivity and salinity obtained at different depths

585   by CTD buoy 2019O2 as part of the MOSAiC Distributed Network, https://doi.org/10.1594/PANGAEA.933928, 2021b.

Hoppmann, M., Kuznetsov, I., Fang, Y.-C., and Rabe, B.: Raw seawater temperature, conductivity and salinity obtained at different depths by CTD buoy 2019O3 as part of the MOSAiC Distributed Network, https://doi.org/10.1594/PANGAEA.933932, 2021c.

Hoppmann, M., Kuznetsov, I., Fang, Y.-C., and Rabe, B.: Raw seawater temperature, conductivity and salinity obtained at different depths by CTD buoy 2019O4 as part of the MOSAiC Distributed Network, https://doi.org/10.1594/PANGAEA.933933, 2021d.

590   Hoppmann, M., Kuznetsov, I., Fang, Y.-C., and Rabe, B.: Raw seawater temperature, conductivity and salinity obtained at different depths by CTD buoy 2019O5 as part of the MOSAiC Distributed Network, https://doi.org/10.1594/PANGAEA.933937, 2021e.

Hoppmann, M., Kuznetsov, I., Fang, Y.-C., and Rabe, B.: Raw seawater temperature, conductivity and salinity obtained at different depths by CTD buoy 2019O6 as part of the MOSAiC Distributed Network, https://doi.org/10.1594/PANGAEA.933941, 2021f.

Hoppmann, M., Kuznetsov, I., Fang, Y.-C., and Rabe, B.: Raw seawater temperature, conductivity and salinity obtained at different depths

595   by CTD buoy 2019O7 as part of the MOSAiC Distributed Network, https://doi.org/10.1594/PANGAEA.933939, 2021g.

Hoppmann, M., Kuznetsov, I., Fang, Y.-C., and Rabe, B.: Raw seawater temperature, conductivity and salinity obtained at different depths by CTD buoy 2019O8 as part of the MOSAiC Distributed Network, https://doi.org/10.1594/PANGAEA.933942, 2021h.

Hoppmann, M., Kuznetsov, I., Fang, Y.-C., and Rabe, B.: Raw seawater temperature, conductivity and salinity obtained with CTD buoys as part of the MOSAiC Distributed Network, https://doi.org/10.1594/PANGAEA.937271, 2021i.

600   Hoppmann, M., Kuznetsov, I., Fang, Y.-C., and Rabe, B.: Processed seawater temperature, conductivity and salinity obtained at different depths by CTD buoy 2019O1 as part of the MOSAiC Distributed Network, https://doi.org/10.1594/PANGAEA.940271, 2022a.

Hoppmann, M., Kuznetsov, I., Fang, Y.-C., and Rabe, B.: Processed seawater temperature, conductivity and salinity obtained at different depths by CTD buoy 2019O2 as part of the MOSAiC Distributed Network, https://doi.org/10.1594/PANGAEA.940298, 2022b.

Hoppmann, M., Kuznetsov, I., Fang, Y.-C., and Rabe, B.: Processed seawater temperature, conductivity and salinity obtained at different depths by CTD buoy 2019O3 as part of the MOSAiC Distributed Network, https://doi.org/10.1594/PANGAEA.940282, 2022c.

Hoppmann, M., Kuznetsov, I., Fang, Y.-C., and Rabe, B.: Processed seawater temperature, conductivity and salinity obtained at different depths by CTD buoy 2019O4 as part of the MOSAiC Distributed Network, https://doi.org/10.1594/PANGAEA.940291, 2022d.

Hoppmann, M., Kuznetsov, I., Fang, Y.-C., and Rabe, B.: Processed seawater temperature, conductivity and salinity obtained at different depths by CTD buoy 2019O5 as part of the MOSAiC Distributed Network, https://doi.org/10.1594/PANGAEA.940301, 2022e.

Hoppmann, M., Kuznetsov, I., Fang, Y.-C., and Rabe, B.: Processed seawater temperature, conductivity and salinity obtained at different depths by CTD buoy 2019O6 as part of the MOSAiC Distributed Network, https://doi.org/10.1594/PANGAEA.940296, 2022f.

Hoppmann, M., Kuznetsov, I., Fang, Y.-C., and Rabe, B.: Processed seawater temperature, conductivity and salinity obtained at different depths by CTD buoy 2019O7 as part of the MOSAiC Distributed Network, https://doi.org/10.1594/PANGAEA.940303, 2022g.

Hoppmann, M., Kuznetsov, I., Fang, Y.-C., and Rabe, B.: Processed seawater temperature, conductivity and salinity obtained at different depths by CTD buoy 2019O8 as part of the MOSAiC Distributed Network, https://doi.org/10.1594/PANGAEA.940304, 2022h.

Hoppmann, M., Kuznetsov, I., Fang, Y.-C., and Rabe, B.: Processed data of CTD buoys 2019O1 to 2019O8 as part of the MOSAiC Distributed Network, https://doi.org/10.1594/PANGAEA.940320, 2022i.

Huang, X., Wang, Z., Zhang, Z., Yang, Y., Zhou, C., Yang, Q., Zhao, W., and Tian, J.: Role of Mesoscale Eddies in Modulating the Semidiurnal Internal Tide: Observation Results in the Northern South China Sea, Journal of Physical Oceanography, 48, 1749–1770, https://doi.org/10.1175/JPO-D-17-0209.1, 2018.

Ilicak, M., Drange, H., Wang, Q., Gerdes, R., Aksenov, Y., Bailey, D., Bentsen, M., Biastoch, A., Bozec, A., Boening, C., Cassou, C., Chassignet, E., Coward, A. C., Curry, B., Danabasoglu, G., Danilov, S., Fernandez, E., Fogli, P. G., Fujii, Y., Griffies, S. M., Iovino, D., Jahn, A., Jung, T., Large, W. G., Lee, C., Lique, C., Lu, J., Masina, S., Nurser, A. J. G., Roth, C., Salas y Melia, D., Samuels, B. L., Spence, P., Tsujino, H., Valcke, S., Voldoire, A., Wang, X., and Yeager, S. G.: An assessment of the Arctic Ocean in a suite of interannual CORE-II simulations. Part III: Hydrography and fluxes, Ocean Modelling, 100, 141–161, https://doi.org/10.1016/j.ocemod.2016.02.004, 2016.

Jackson, K., Wilkinson, J., Maksym, T., Beckers, J., Haas, C., Meldrum, D., and Mackenzie, D.: A Novel and Low Cost Sea Ice Mass Balance Buoy, Journal of Atmospheric and Oceanic Technology, https://doi.org/10.1175/jtech-d-13-00058.1, 2013.

Jakobsson, M., Mayer, L. A., Bringensparr, C., Castro, C. F., Mohammad, R., Johnson, P., Ketter, T., Accettella, D., Amblas, D., An, L., Arndt, J. E., Canals, M., Casamor, J. L., Chauché, N., Coakley, B., Danielson, S., Demarte, M., Dickson, M.-L., Dorschel, B., Dowdeswell, J. A., Dreutter, S., Fremand, A. C., Gallant, D., Hall, J. K., Hehemann, L., Hodnesdal, H., Hong, J., Ivaldi, R., Kane, E., Klaucke, I., Krawczyk, D. W., Kristoffersen, Y., Kuipers, B. R., Millan, R., Masetti, G., Morlighem, M., Noormets, R., Prescott, M. M., Rebesco, M., Rignot, E., Semiletov, I., Tate, A. J., Travaglini, P., Velicogna, I., Weatherall, P., Weinrebe, W., Willis, J. K., Wood, M., Zarayskaya, Y., Zhang, T., Zimmermann, M., and Zinglersen, K. B.: The International Bathymetric Chart of the Arctic Ocean Version 4.0, Scientific Data, 7, 176, https://doi.org/10.1038/s41597-020-0520-9, 2020.

Jochum, M. and Murtugudde, R., eds.: Physical Oceanography: Developments Since 1950, Springer-Verlag New York, 1 edn., https://doi.org/10.1007/0-387-33152-2, 2006.

Kaiser, P., Hagen, W., von Appen, W.-J., Niehoff, B., Hildebrandt, N., and Auel, H.: Effects of a submesoscale oceanographic filament on zooplankton dynamics in the Arctic marginal ice zone, Frontiers in Marine Research, 8, https://doi.org/10.3389/fmars.2021.625395, 2021.

Kikuchi, T., Inoue, J., and Langevin, D.: Argo-type profiling float observations under the Arctic multiyear ice, Deep-Sea Res. I, 54, 1675–1686, https://doi.org/10.1016/j.dsr.2007.05.011, 2007.

Koenig, Z., Provost, C., Villacieros-Robineau, N., Sennechael, N., and Meyer, A.: Winter ocean-ice interactions under thin sea ice observed by IAOOS platforms during N-ICE2015: Salty surface mixed layer and active basal melt, Journal of Geophysical Research: Oceans, 121, 7898–7916, https://doi.org/10.1002/2016JC012195, 2016.

645 Krumpen, T., Birrien, F., Kauker, F., Rackow, T., von Albedyll, L., Angelopoulos, M., Belter, H. J., Bessonov, V., Damm, E., Dethloff, K., Haapala, J., Haas, C., Harris, C., Hendricks, S., Hoelemann, J., Hoppmann, M., Kaleschke, L., Karcher, M., Kolabutin, N., Lei, R., Lenz, J., Morgenstern, A., Nicolaus, M., Nixdorf, U., Petrovsky, T., Rabe, B., Rabenstein, L., Rex, M., Ricker, R., Rohde, J., Shimanchuk, E., Singha, S., Smolyanitsky, V., Sokolov, V., Stanton, T., Timofeeva, A., Tsamados, M., and Watkins, D.: The MOSAiC ice floe: sediment-laden survivor from the Siberian shelf, The Cryosphere, 14, 2173–2187, https://doi.org/10.5194/tc-14-2173-2020, 2020.

650 Lee, C. M., Thomson, J., Team, M. I. Z., and Team, A. S. S.: An Autonomous Approach to Observing the Seasonal Ice Zone in the Western Arctic, Oceanography, 30, 56–68, https://doi.org/10.5670/oceanog.2017.222, 2017.

Lévy, M., Iovino, D., Resplandy, L., Klein, P., Madec, G., Tréguier, A.-M., Masson, S., and Takahashi, K.: Large-scale impacts of submesoscale dynamics on phytoplankton: Local and remote effects, Ocean Modelling, 43-44, 77–93, https://doi.org/10.1016/j.ocemod.2011.12.003, 2012.

655 Lévy, M., Franks, P., and Smith, K. S.: The role of submesoscale currents in structuring marine ecosystems, Nature Communications, 9, https://doi.org/10.1038/s41467-018-07059-3, 2018.

Mahadevan, A.: The Impact of Submesoscale Physics on Primary Productivity of Plankton, Annual Review of Marine Science, 8, 161–184, https://doi.org/10.1146/annurev-marine-010814-015912, 2016.

Mahadevan, A., Tandon, A., and Ferrari, R.: Rapid changes in mixed layer stratification driven by submesoscale instabilities and winds, 660 Journal of Geophysical Research: Oceans, 115, 1–12, https://doi.org/10.1029/2008JC005203, 2010.

Manley, T. O. and Hunkins, K.: Mesoscale eddies of the Arctic Ocean, Journal of Geophysical Research: Oceans, 90, 4911–4930, https://doi.org/doi:10.1029/JC090iC03p04911, 1985.

Manucharyan, G. E. and Thompson, A. F.: Submesoscale Sea Ice-Ocean Interactions in Marginal Ice Zones, Journal of Geophysical Research: Oceans, 122, 9455–9475, https://doi.org/10.1002/2017JC012895, 2017.

665 Manucharyan, G. E. and Timmermans, M.-L.: Generation and Separation of Mesoscale Eddies from Surface Ocean Fronts, Journal of Physical Oceanography, 43, 2545–2562, https://doi.org/10.1175/JPO-D-13-094.1, 2013.

Marcinko, C. L., Martin, A. P., and Allen, J. T.: Characterizing horizontal variability and energy spectra in the Arctic Ocean halocline, Journal of Geophysical Research: Oceans, 120, 436–450, https://doi.org/10.1002/2014JC010381, 2015.

McDougall, T. and Barker, P.: Getting Started with TEOS-10 and the Gibbs Seawater (GSW) Oceanographic Toolbox: Version 3.0, 670 SCOR/IAPSO WG127, 2011.

McGillicuddy, D. J.: Mechanisms of Physical-Biological-Biogeochemical Interaction at the Oceanic Mesoscale, Annual Review of Marine Science, 8, 125–159, https://doi.org/10.1146/annurev-marine-010814-015606, 2016.

McWilliams, J. C.: Maps from the Mid-Ocean Dynamics Experiment: Part I. Geostrophic Streamfunction, Journal of Physical Oceanography, 6, 810–827, https://doi.org/10.1175/1520-0485(1976)006<0810:MFTMOD>2.0.CO;2, 1976.

675 McWilliams, J. C.: Submesoscale currents in the ocean, Proceedings of the Royal Society of London A, 472, https://doi.org/10.1098/rspa.2016.0117, 2016.

Nicolaus, M., Hoppmann, M., Arndt, S., Hendricks, S., Katlein, C., Nicolaus, A., Rossmann, L., Schiller, M., and Schwegmann, S.: Snow Depth and Air Temperature Seasonality on Sea Ice Derived From Snow Buoy Measurements, Frontiers in Marine Science, 8, https://doi.org/10.3389/fmars.2021.655446, 2021a.

680 Nicolaus, M., Riemann-Campe, K., Hutchings, J. K., Granskog, M. A., Krishfield, R. A., Lei, R., Li, T., Hoppmann, M., and Rabe, B.: Drift trajectories of the main sites of the Distributed Network of MOSAiC 2019/2020, PANGAEA, https://doi.org/10.1594/PANGAEA.937204, 2021b.

Nicolaus, M., Perovich, D. K., Spreen, G., Granskog, M. A., von Albedyll, L., Angelopoulos, M., Anhaus, P., Arndt, S., Belter, H. J., Bessonov, V., Birnbaum, G., Brauchle, J., Calmer, R., Cardellach, E., Cheng, B., Clemens-Sewall, D., Dadic, R., Damm, E., de Boer, 685 G., Demir, O., Dethloff, K., Divine, D. V., Fong, A. A., Fons, S., Frey, M. M., Fuchs, N., Gabarró, C., Gerland, S., Goessling, H. F., Gradinger, R., Haapala, J., Haas, C., Hamilton, J., Hannula, H.-R., Hendricks, S., Herber, A., Heuzé, C., Hoppmann, M., Høyland, K. V., Huntemann, M., Hutchings, J. K., Hwang, B., Itkin, P., Jacobi, H.-W., Jaggi, M., Jutila, A., Kaleschke, L., Katlein, C., Kolabutin, N., Krampe, D., Kristensen, S. S., Krumpen, T., Kurtz, N., Lampert, A., Lange, B. A., Lei, R., Light, B., Linhardt, F., Liston, G. E., Loose, B., Macfarlane, A. R., Mahmud, M., Matero, I. O., Maus, S., Morgenstern, A., Naderpour, R., Nandan, V., Niubom, A., Oggier, M., 690 Oppelt, N., Pätzold, F., Perron, C., Petrovsky, T., Pirazzini, R., Polashenski, C., Rabe, B., Raphael, I. A., Regnery, J., Rex, M., Ricker, R., Riemann-Campe, K., Rinke, A., Rohde, J., Salganik, E., Scharien, R. K., Schiller, M., Schneebeli, M., Semmling, M., Shimanchuk, E., Shupe, M. D., Smith, M. M., Smolyanitsky, V., Sokolov, V., Stanton, T., Stroeve, J., Thielke, L., Timofeeva, A., Tonboe, R. T., Tavri, A., Tsamados, M., et al.: Overview of the MOSAiC expedition: Snow and sea ice, Elementa: Science of the Anthropocene, 10, 000 046, https://doi.org/10.1525/elementa.2021.000046, 2022.

695 Nixdorf, U., Dethloff, K., Rex, M., Shupe, M., Sommerfeld, A., Perovich, D. K., Nicolaus, M., Heuzé, C., Rabe, B., Loose, B., Damm, E., Gradinger, R., Fong, A., Maslowski, W., Rinke, A., Kwok, R., Spreen, G., Wendisch, M., Herber, A., Hirsekorn, M., Mohaupt, V., Frickenhaus, S., Immerz, A., Weiss-Tuider, K., König, B., Mengedoht, D., Regnery, J., Gerchow, P., Ransby, D., Krumpen, T., Morgenstern, A., Haas, C., Kanzow, T., Rack, F. R., Saitzev, V., Sokolov, V., Makarov, A., Schwarze, S., Wunderlich, T., Wurr, K., and Boetius, A.: MOSAiC Extended Acknowledgement, https://doi.org/10.5281/zenodo.5541624, 2021.

700 Nurser, A. J. G. and Bacon, S.: The Rossby radius in the Arctic Ocean, Ocean Science, 10, 967–975, https://doi.org/10.5194/os-10-967-2014, 2014.

Ocean University of China: The Drift-Towing Ocean Profiler, http://coas.ouc.edu.cn/pogoc/2021/0713/c9714a342585/page.htm, 2021.

Polyakov, I. V., Pnyushkov, A. V., Rember, R., Padman, L., Carmack, E. C., and Jackson, J. M.: Winter Convection Transports Atlantic Water Heat to the Surface Layer in the Eastern Arctic Ocean, JOURNAL OF PHYSICAL OCEANOGRAPHY, 43, 2142–2155, 705 https://doi.org/10.1175/JPO-D-12-0169.1, 2013.

Porter, M., Henley, S. F., Orkney, A., Bouman, H. A., Hwang, B., Dumont, E., Venables, E. J., and Cottier, F.: A Polar Surface Eddy Obscured by Thermal Stratification, Geophysical Research Letters, 47, e2019GL086 281, https://doi.org/https://doi.org/10.1029/2019GL086281, 2020.

Rabe, B., Heuzé, C., Regnery, J., Aksenov, Y., Allerholt, J., Athanase, M., Bai, Y., Basque, C., Bauch, D., Baumann, T. M., Chen, D., Cole, 710 S. T., Craw, L., Davies, A., Damm, E., Dethloff, K., Divine, D. V., Doglioni, F., Ebert, F., Fang, Y.-C., Fer, I., Fong, A. A., Gradinger, R., Granskog, M. A., Graupner, R., Haas, C., He, H., He, Y., Hoppmann, M., Janout, M., Kadko, D., Kanzow, T., Karam, S., Kawaguchi, Y., Koenig, Z., Kong, B., Krishfield, R. A., Krumpen, T., Kuhlmey, D., Kuznetsov, I., Lan, M., Laukert, G., Lei, R., Li, T., Torres-Valdés, S., Lin, L., Lin, L., Liu, H., Liu, N., Loose, B., Ma, X., McKay, R., Mallet, M., Mallett, R. D. C., Maslowski, W., Mertens, C., Mohrholz, V., Muilwijk, M., Nicolaus, M., O'Brien, J. K., Perovich, D., Ren, J., Rex, M., Ribeiro, N., Rinke, A., Schaffer, J., Schuffenhauer, I., 715 Schulz, K., Shupe, M. D., Shaw, W., Sokolov, V., Sommerfeld, A., Spreen, G., Stanton, T., Stephens, M., Su, J., Sukhikh, N., Sundfjord, A., Thomisch, K., Tippenhauer, S., Toole, J. M., Vredenborg, M., Walter, M., Wang, H., Wang, L., Wang, Y., Wendisch, M., Zhao, J.,

Zhou, M., and Zhu, J.: Overview of the MOSAiC expedition: Physical oceanography, Elementa: Science of the Anthropocene, 10, 00 062, https://doi.org/10.1525/elementa.2021.00062, 2022.

Shupe, M. D., Rex, M., Blomquist, B., Persson, P. O. G., Schmale, J., Uttal, T., Althausen, D., Angot, H., Archer, S., Bariteau, L., Beck, I., Bilberry, J., Bucci, S., Buck, C., Boyer, M., Brasseur, Z., Brooks, I. M., Calmer, R., Cassano, J., Castro, V., Chu, D., Costa, D., Cox, C. J., Creamean, J., Crewell, S., Dahlke, S., Damm, E., de Boer, G., Deckelmann, H., Dethloff, K., Dütsch, M., Ebell, K., Ehrlich, A., Ellis, J., Engelmann, R., Fong, A. A., Frey, M. M., Gallagher, M. R., Ganzeveld, L., Gradinger, R., Graeser, J., Greenamyer, V., Griesche, H., Griffiths, S., Hamilton, J., Heinemann, G., Helmig, D., Herber, A., Heuzé, C., Hofer, J., Houchens, T., Howard, D., Inoue, J., Jacobi, H.-W., Jaiser, R., Jokinen, T., Jourdan, O., Jozef, G., King, W., Kirchgaessner, A., Klingebiel, M., Krassovski, M., Krumpen, T., Lampert, A., Landing, W., Laurila, T., Lawrence, D., Lonardi, M., Loose, B., Lüpkes, C., Maahn, M., Macke, A., Maslowski, W., Marsay, C., Maturilli, M., Mech, M., Morris, S., Moser, M., Nicolaus, M., Ortega, P., Osborn, J., Pätzold, F., Perovich, D. K., Petäjä, T., Pilz, C., Pirazzini, R., Posman, K., Powers, H., Pratt, K. A., Preußer, A., Quéléver, L., Radenz, M., Rabe, B., Rinke, A., Sachs, T., Schulz, A., Siebert, H., Silva, T., Solomon, A., Sommerfeld, A., et al.: Overview of the MOSAiC expedition—Atmosphere, Elementa: Science of the Anthropocene, 10, 00 060, https://doi.org/10.1525/elementa.2021.00060, 2022.

Smith, K. S.: The geography of linear baroclinic instability in Earth's oceans, Journal of Marine Research, 65, 655–683, https://doi.org/10.1357/002224007783649484, 2007.

Stedmon, C. A., Amon, R. M. W., Bauch, D., Bracher, A., Gonçalves-Araujo, R., Hoppmann, M., Krishfield, R. A., Laney, S., Rabe, B., Reader, H. E., and et al.: Insights into Water Mass Circulation and Origins in the Central Arctic Ocean from in-situ Dissolved Organic Matter Fluorescence, Journal of Geophysical Research: Oceans, 126, 27, https://doi.org/10.1029/2021JC017407, 2021.

Steele, M.: UpTempO buoys deployed in the Arctic Ocean in 2017, Arctic Data Center, https://doi.org/10.18739/A2GB1XG6P, 2017.

Thomas, L. N.: Destruction of Potential Vorticity by Winds, Journal of Physical Oceanography, 35, 2457–2466, https://doi.org/10.1175/JPO2830.1, 2005.

Thomas, L. N., Tandon, A., and Mahadevan, A.: Submesoscale Processes and Dynamics, https://doi.org/doi:10.1029/177GM04, 2008.

Timmermans, M.-L. and Marshall, J.: Understanding Arctic Ocean Circulation: A Review of Ocean Dynamics in a Changing Climate, Journal of Geophysical Research: Oceans, 125, https://doi.org/10.1029/2018JC014378, 2020.

Timmermans, M.-L., Cole, S., and Toole, J.: Horizontal Density Structure and Restratification of the Arctic Ocean Surface Layer, Journal of Physical Oceanography, 42, 659–668, https://doi.org/10.1175/JPO-D-11-0125.1, 2012.

Toole, J., Krishfield, R., Proshutinsky, A., Ashjian, C., Doherty, K., Frye, D., Hammar, T., Kemp, J., Peters, D., Timmermans, M.-L., von der Heydt, K., Packard, G., and Shanahan, T.: Ice-tethered profilers sample the upper Arctic Ocean, Eos, Transactions American Geophysical Union, 87, 434–438, https://doi.org/10.1029/2006EO410003, 2006.

UNESCO-IOC: Ocean Data Standards Volume 3. Recommendation for a Quality Flag Scheme for the Exchange of Oceanographic and Marine Meteorological Data, https://doi.org/10.25607/OBP-6, 2013.

von Appen, W. J., Wekerle, C., Hehemann, L., Schourup-Kristensen, V., Konrad, C., and Iversen, M. H.: Observations of a Submesoscale Cyclonic Filament in the Marginal Ice Zone, Geophysical Research Letters, 45, 6141–6149, https://doi.org/10.1029/2018GL077897, 2018.

von Appen, W.-J., Baumann, T., Janout, M., Koldunov, N., Lenn, Y.-D., Pickart, R., Scott, R., and Wang, Q.: Eddies and the Distribution of Eddy Kinetic Energy in the Arctic Ocean, Oceanography, 35, https://doi.org/10.5670/oceanog.2022.122, 2022.

Wang, Q., Koldunov, N. V., Danilov, S., Sidorenko, D., Wekerle, C., Scholz, P., Bashmachnikov, I. L., and Jung, T.: Eddy Kinetic Energy in the Arctic Ocean From a Global Simulation With a 1-km Arctic, Geophysical Research Letters, 47, 1–11, https://doi.org/10.1029/2020GL088550, 2020.

755 Wessel, P. and Smith, W. H. F.: A global, self-consistent, hierarchical, high-resolution shoreline database, Journal of Geophysical Research: Solid Earth, 101, 8741–8743, https://doi.org/10.1029/96JB00104, 1996.

Zhang, X., Dai, H., Zhao, J., and Yin, H.: Generation mechanism of an observed submesoscale eddy in the Chukchi Sea, Deep-Sea Research Part I: Oceanographic Research Papers, 148, 80–87, https://doi.org/10.1016/j.dsr.2019.04.015, 2019.

Zhao, M., Timmermans, M.-L., Cole, S., Krishfield, R., Proshutinsky, A., and Toole, J.: Characterizing the eddy field in the Arctic Ocean
760 halocline, Journal of Geophysical Research: Oceans, 119, 8800–8817, https://doi.org/10.1002/2014JC010488, 2014.

Zhao, M., Timmermans, M.-L., Cole, S., Krishfield, R., and Toole, J.: Evolution of the eddy field in the Arctic Ocean's Canada Basin, 2005-2015, Geophysical Research Letters, 43, 8106–8114, https://doi.org/10.1002/2016GL069671, 2016.

Appendix A: Additional Figures & Tables
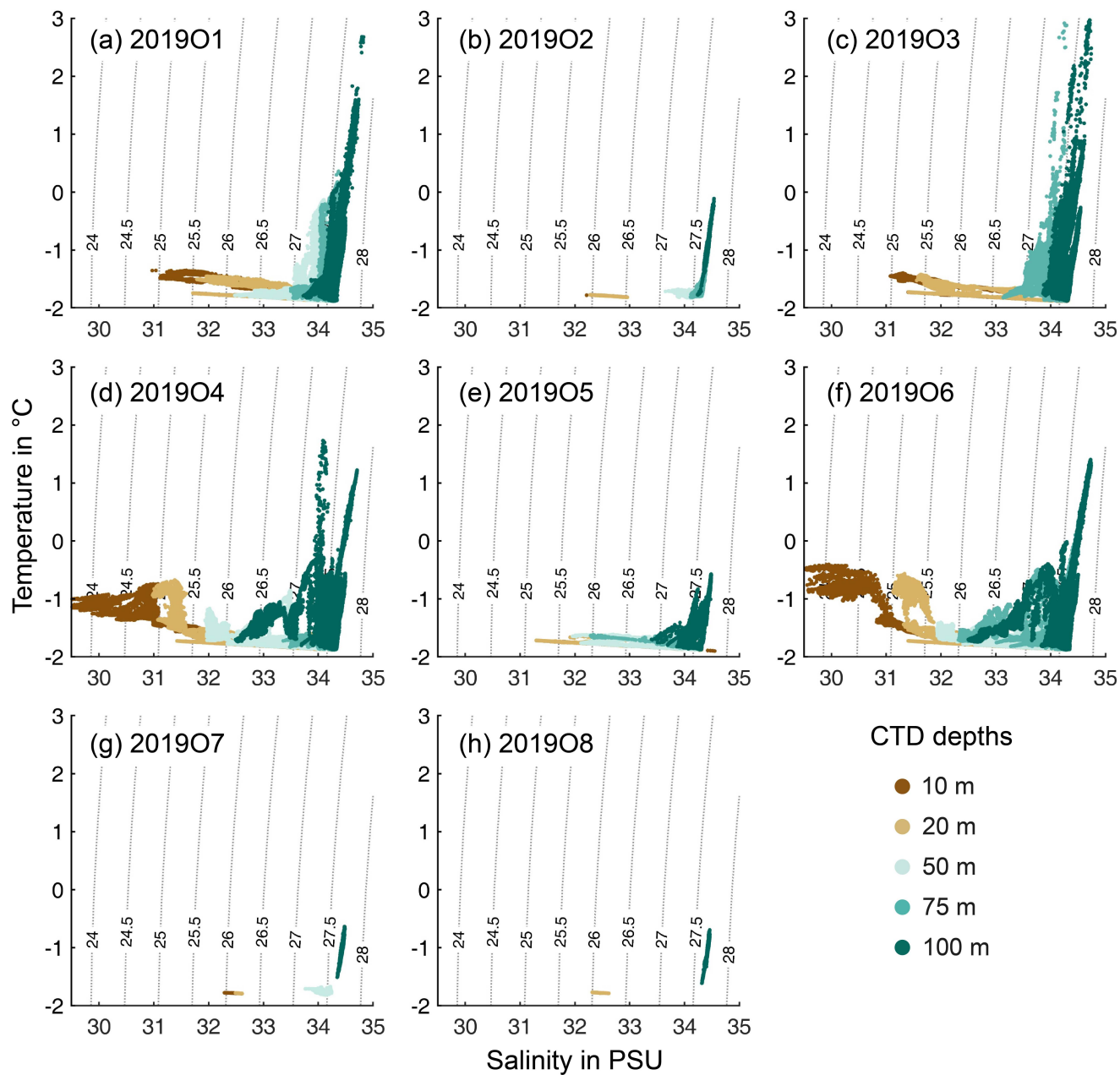
Figure A1. T-S diagrams based on the processed datasets collected by all eight buoys during their drift through the central Arctic as part of the MOSAiC Distributed Network. Note that these diagrams strongly depend on the operation lifetime of the corresponding buoy.

Table A1. Comparison of SST-CTD profiles with buoy measurements for validation.

Station	Event (date)	Depth (m)	Temperature diff.	Salinity diff.
2019O1	PS122/3_38-101	10	0.0	-0.012
	2020-05-02	20	-0.002	-0.012
		50	0.003	-0.006
		75	-0.001	-0.012
		100	-0.004	-0.017
2019O3	PS122/3_37-119	10	-0.002	-0.002
	2020-04-26	20	-0.001	0.004
		75	-0.001	-0.016
		100	-0.002	-0.005
2019O4	PS122/3_38-102	10	0.0	-0.002
	2020-05-02	20	-0.001	-0.004
		50	-0.001	0.005
		100	-0.001	-0.003
2019O5	PS122/3_37-120	10	-0.002	-0.002
	2020-04-26	20	-0.001	-0.001
		50	-0.004	-0.002
		100	-0.004	-0.005
2019O6	PS122/3_38-103	9	-0.003	-0.006
	2020-05-02	19	-0.003	-0.001
		50	-0.004	-0.004
		75	-0.004	-0.002
		100	-0.002	0.001